e-Newsletter n°1

June 2007

Available at http://www.ist-brighter.eu

WWW.BRIGHTER.EU

World Wide Welfare: High-Brightness Semiconductor Lasers for Generic Use

WWW.BRIGHTER.EU is an integrated project supported by the European Commission's Information Society Technologies programme

CONTENT

EDITORIAL

Welcome to the 1st e-Newsletter of our new 3 year integrated project WWW.BRIGHTER.EU, which began in October 2006. This integrated project builds upon our previous successful WWW.BRIGHT.EU project, in which we published our first series of three e-Newsletters.

Throughout the next 3 years we will be publishing project e-Newsletters twice yearly to keep you up to date with the latest developments of our project.

We hope you will enjoy reading this e-Newsletter.

The Editors

Steve Bull
University of Nottingham
steve.bull@nottingham.ac.uk

Myriam Oudart
Alcatel Thales III-V lab
myriam.oudart@3-5lab.fr

Eric Larkins
University of Nottingham
eric.larkins@nottingham.ac.uk

GREETINGS FROM THE PROJECT COORDINATOR

Dear Reader,

Michel Krakowski
Project Coordinator
Alcatel Thales III-V Lab
michel.krakowski@3-5lab.fr

Welcome to the first semi-annual e-Newsletter of our new EC-IST Project ***World Wide Welfare: High-Brightness Semiconductor Lasers for Generic Use – "WWW.BRIGHTER.EU"***, an Integrated Project on high-brightness laser diode technologies and their applications, which builds upon the successes of our previous project *WWW.BRIGHT.EU* (2004-06).

Since the efficiency of optical fibre transmission was demonstrated some 30 years ago, the demand for high-brightness sources and their range of applications has increased continuously. High-brightness laser diodes are a key enabling technology for the information society of tomorrow, especially in healthcare, communications, entertainment, environment and security.

The WWW.BRIGHTER.EU Consortium of 23 partners is pursuing a long-term vision aimed at pushing the limits of current laser diode technology towards higher brightness and also stimulating the development of new applications and markets, such as biophotonics (photodynamic therapy, fluorescence diagnosis) and entertainment (laser displays, laser projectors).

Our approach mobilises the expertise of the main European partners in laser diode core technology and couples this with highly innovative optical technologies. Industrialisation issues are being explored through packaging and reliability studies. Commercial and exploitation issues are covered by several groups within the consortium with access to the relevant markets in our targeted application areas.

More about the project objectives and partners can be found over the next few pages. This newsletter also contains four extended articles. Two applications topics cover the use of lasers in wireless communications systems and the important process of frequency-doubling diode lasers. Two technical articles discuss firstly the design of high-brightness tapered lasers and then laser bar degradation by investigating the performance of the emitters and interactions between them – the so-called "by-emitter" degradation analysis method.

continued…

The WWW.BRIGHTER.EU Consortium is pleased to announce that it will be hosting a special workshop session ***"High-Brightness Laser Sources"*** at the forthcoming **CLEO-Europe Conference** in Munich. Later in the year, the Consortium is also planning a special session ***"Defects in Devices"*** as part of the **DRIP-XII Conference** in Berlin. Further information on both of these special events by the Consortium can be found on pages 7 – 9. Details of other conferences and exhibitions throughout the year where members of the Consortium will be presenting / exhibiting are included on page 10.

We hope that you find our e-Newsletter interesting and informative. If you are interested in exploring the advantages offered by high-brightness lasers for your applications or simply wish to comment upon or discuss any of the issues touched upon in this e-Newsletter in greater depth, please do not hesitate to contact us or visit our website at http://www.ist-brighter.eu.

WWW.BRIGHTER.EU PROJECT OVERVIEW

Laser diodes offer high output power, compactness, robustness and mass production capabilities. However, their use in many domains such as healthcare, communications, entertainment, environment and security is often limited by the difficulty in reaching satisfactory performances on power and beam quality simultaneously. The term "high brightness" indicates exactly the capability of a high-power laser diode to provide high beam quality. The brightness directly governs the performance of systems, such as the transmission span of an optical data link, the reliability of a diagnosis in fluorescence imaging of cancer or the resolution of a laser projection display.

The WWW.BRIGHTER.EU project is building upon the Consortium's successful WWW.BRIGHT.EU project, which was completed in 2006. Using the know-how and results from this previous project, WWW.BRIGHTER.EU offers a more comprehensive and ambitious approach, taking into account the recent market developments and evolution of the state-of-the-art. In some aspects, WWW.BRIGHTER.EU is continuing and strengthening the efforts deployed in the earlier project, but at the same time it is also introducing new concepts and applications that were not previously targeted.

PROJECT FACTS

Start Date: 1st Oct. 2006
Duration: 36 Months
Project Cost: 16.26 M€
EC Funding: 9.70 M€
Consortium: 23 Partners
7 Industrial (3 SME's)
9 Research Centres
7 Universities

Main Focus of WWW.BRIGHT.EU (2004-2006)

- Development of diode lasers at 405, 635, 650, 810, 915 and 980nm
- Development of reliable technologies for coupling into both 200µm and 50µm fibres
- Demonstration and first assessment of external cavity approaches:
    - Tunable lasers
    - Four-wave mixing diode laser cavities
    - Self-organising cavities
    - Wavelength multiplexing
- Healthcare applications:
    - Fluorescence diagnosis at 405nm using frequency-doubled 810nm lasers
    - Photodynamic therapy with the photosensitizer ALA activated at 635nm
    - Photodynamic therapy with the photosensitizer Foscan activated at 652nm

Applications Targeted in WWW.BRIGHTER.EU (2006-2009)

Healthcare: Full validation of PDT lasers (with clinical tests), diagnostic and monitoring techniques for the assessment of PDT progress, 340nm fluorescence imaging / diagnosis

Telecoms: Full validation of the Raman amplifier, inclusion of new industrial partner for the component manufacturing and exploitation

Wireless Communications: Assessment of the improvement linked to the use of 980nm and Esaki junction lasers

Displays: New application targeted in WWW.BRIGHTER.EU that will benefit from the synergies with the 635nm and 650nm lasers developed for PDT and from the frequency-doubling techniques developed for fluorescence diagnosis

Security & Environment: Second new area targeted in WWW.BRIGHTER.EU that will benefit from the synergies with lasers developed for Raman amplification

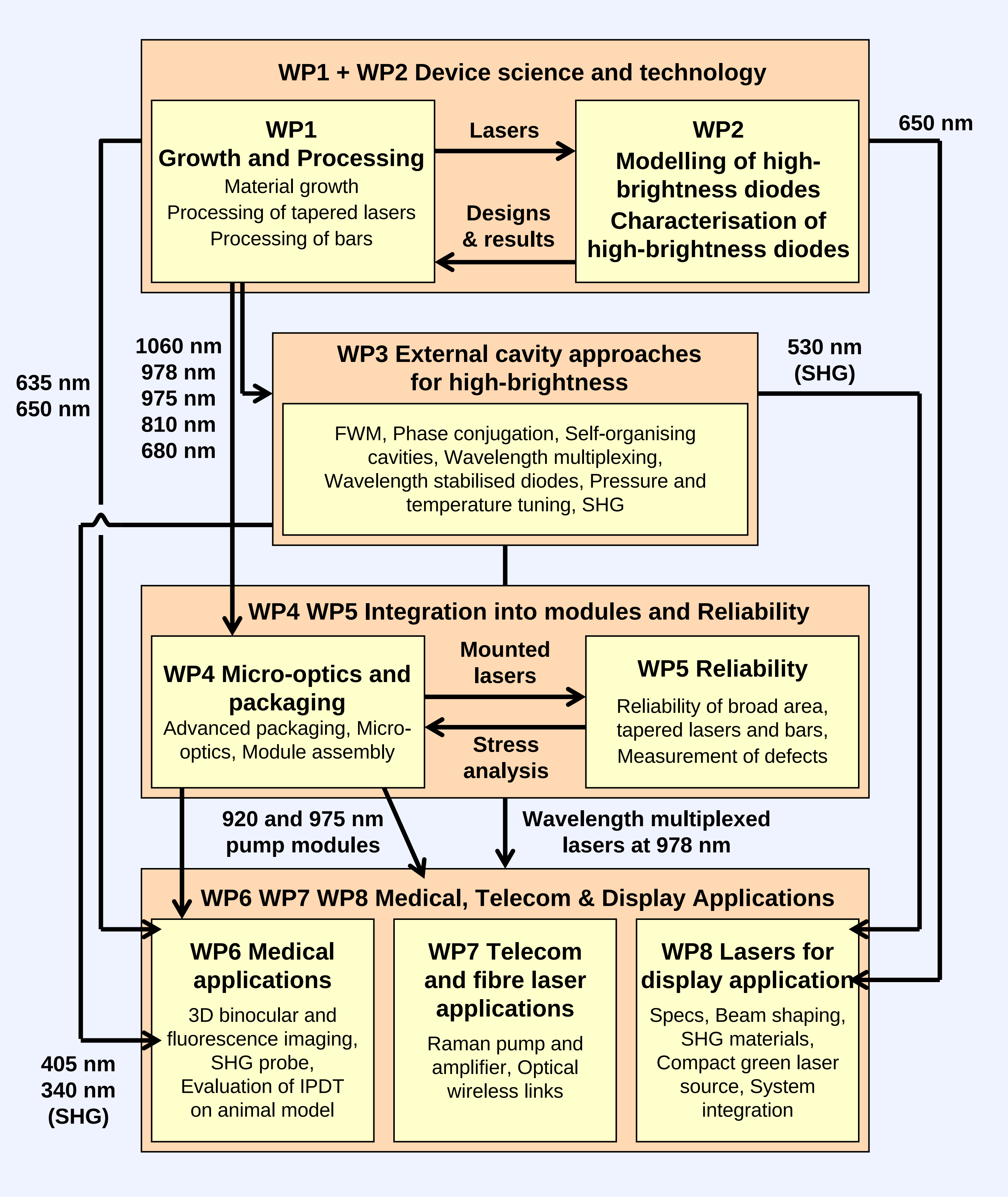

Simplified flowchart representation of the WWW.BRIGHTER.EU project

WWW.BRIGHTER.EU PROJECT CONSORTIUM

The table below lists the Consortium partners. A brief description of each partner's main responsibility within the project is given. Further information on the individual partners can be found in their respective partner profiles.

No.	Partner Name & *Main Responsibilities*	Acronym	Country
1	Alcatel-Thales III-V LAB ***Design, growth, fabrication & characterisation of high-brightness laser sources***	III-V LAB	France
2	Biolitec AG ***Design and implementation of medical laser systems for PDT and surgery***	BIOLITEC	Germany
3	Lund University ***Tissue fluorescence monitoring, Clinical study protocols***	LLC	Sweden
4	Institute of Communication and Computer Systems ***3D fluorescence imaging system for PDT monitoring, Clinical study protocols***	ICCS	Greece
5	Risoe National Laboratory ***FWM laser cavities, External feedback lasers, Wavelength multiplexing***	RISOE	Denmark
6	OSRAM Opto Semiconductors GmbH ***Red-emitting laser bars at 635nm, Evaluation of lasers for display applications***	OSRAM	Germany
7	University of Cambridge ***Modelling, Post-processing using FIBE, Free-space communication systems***	CAM	UK
8	Keopsys ***Realisation of cladding-pumped EDFA's and Raman amplifiers***	KEO	France
9	Alcatel-CIT ***Design and realisation of cladding-pumped EDFA's and Raman amplifiers***	ALCATEL	France
10	Institut National d'Optique ***Micro-optics, Laser systems for pollutant detection & security applications***	INO	Canada
11	Bayerische Julius-Maximilians Universität Würzburg ***Realisation of tapered lasers with gratings for wavelength stabilisation***	UWUERZ	Germany
12	Fisba Optik AG ***Development & production of micro-optics, Module development & assembly***	FISBA	Switzerland
13	Rainbow Photonics AG ***Evaluation of non-linear crystals, Frequency doubling to 340 and 405nm***	RB	Switzerland
14	Thales Research and Technology ***Material characterisation, Reliability studies, Multiplexed external cavity lasers***	TRT	France
15	Universidad Politécnica de Madrid ***Modelling of high-brightness and high wall-plug efficiency laser diodes***	UPM	Spain
16	Ferdinand-Braun-Institute, Forschungsverbund Berlin e.V. ***Red-emitting laser bars at 650nm, Tapered lasers at 810 and 1060nm***	FBH	Germany
17	Fraunhofer-Gesellschaft (ILT, Aachen & IAF, Freiburg) ***Tapered lasers/amplifiers at 975 & 1060nm, Advanced packaging & modules***	FHG	Germany
18	Instytut Wysokich Cisnien PAN ***Temperature and pressure tunable lasers***	UNIPRESS	Poland
19	Universität Kassel ***Fabrication of high quality quantum dot material at 920 and 1060nm***	UKAS	Germany
20	Centre National de la Recherche Scientifique ***Self-organising cavity lasers, Extended cavity lasers with holograms & gratings***	LCFIO	France
21	Max-Born-Institute, Forschungsverbund Berlin e.V. ***Investigation of strain and defects in laser diodes, Reliability studies***	MBI	Germany
22	Tyndall National Institute ***Modelling and realisation of slab-coupled optical waveguide lasers (SCOWLs)***	TYN	Ireland
23	University of Nottingham ***Modelling external cavity lasers, Intracavity characterisation, Reliability studies***	UNOTT	UK

WWW.BRIGHTER.EU WORKSHOP

Workshop at the World of Photonics Congress and Laser2007 Fair
18th June 2007 - Munich

High Brightness Laser Sources

4 SESSIONS

- HB Laser technology
- Packaging, Micro-optics and Reliability
- Frequency doubled lasers
- Medical, Telecom and Display applications

Organizing Institutions

Alcatel Thales 3-5 Lab, University of Nottingham
Fraunhofer Institute ILT, Risø National Laboratory DTU
Biolitec, Ferdinand Braun Institute
University of Cambridge

Registration: *workshop@ist-brighter.eu*

A PROJECT SUPPORTED BY THE EUROPEAN COMMISSION
www.ist-brighter.eu
(www.bright-eu.org)

Workshop Program

Workshop Introduction and Welcome (10:30 – 10:35)

10:30 **Introduction to WWW.BRIGHTER.EU**
Michel Krakowski – ***Alcatel-Thales III-V Lab***

High-Brightness Laser Technology (10:35 – 11:45)

10:35 **External cavities for controlling spatial & spectral properties of SC lasers**
Jean-Pierre Huignard – ***Thales Research and Technology***

10:45 **Reliable high-power red-emitting laser diodes**
Bernd Sumpf – ***Ferdinand Braun Institute***

10:55 **Wavelength stabilised high-power quantum dot lasers**
Hans Peter Reithmaier – ***University of Kassel***

11:05 **Quantum dot lasers & new device concepts for high-brightness applications**
Dieter Bimberg / Nikolai Ledentsov – ***Technical University of Berlin***

11:25 **High-power laser for surgical applications (cutting and ablation)**
Ronald Sroka – ***LFL Munich***

Break

Packaging, Micro-Optics and Reliability (12:05 – 12:45)

12:05 **Micro-optics and fibre coupling of high-brightness laser bars**
Martin Forrer – ***FISBA Optik***

12:15 **How to measure packaging-induced strain in high-brightness diode lasers?**
Jens Tomm – ***Max Born Institute***

12:25 **High-power laser modules and their applications**
Jörg Neukum – ***DILAS***

Break

Frequency-Doubled Lasers (14:00 – 14:50)

14:00 **Second harmonic generation of external cavity tapered diode lasers**
Ole Bjarlin Jensen – ***Risoe National Laboratory***

14:10 **High-power Semiconductor VECSELs**
Anne Tropper – ***University of Southampton***

14:30 **ps applications of diode lasers**
Ranier Erdmann – ***Picoquant***

Break

Medical, Telecom and Display Applications (15:10 – 17:00)

15:10 **Fluorescence diagnostics in medicine - there is a need for improved light sources**
Stefan Andersson-Engels – ***Lund University***

15:20 **Diode lasers for photodynamic therapy**
Tilmann Trebst – ***Biolitec***

15:30 **Laser-induced fluorescence spectroscopy and molecular imaging as tools for tumour detection in vivo**
Bernd Ebert – ***Physikalisch-Technische Bundesanstalt***

15:50 **Shrinking optically-pumped frequency-doubled green semiconductor lasers to fit into tiny laser projectors**
Michael Kühnelt – ***OSRAM Opto Semiconductors***

16:10 **Laser display markets, technologies and requirements**
Holger Mönch – ***Philips Research Laboratories***

16:30 **Fibre amplifiers and pumping technologies**
Mark Le Flohic – ***Keopsys***

16:40 **Making use of brighter lasers - Optical amplifiers in current and future WDM systems**
Jörg Peter Ebers – ***Ericsson***

Note: The above program is subject to change at the discretion of the workshop organisers.

DRIP-XII CONFERENCE – SEPTEMBER 2007

Two WWW.BRIGHTER.EU partners, the Max-Born-Institute (MBI) and the Ferdinand-Braun-Institute (FBH), will jointly host “DRIP-XII – The International Conference on Defects – Recognition, Imaging and Physics in Semiconductors”, which will be held September 9th – 13th 2007 in Berlin, Germany.

The DRIP conference is an established international conference series with a tradition of more than 20 years, which brings together the leading scientists in the fields of semiconductor physics and technology.

Conference Topics

- New frontiers of atomic-scale-defect assessment using nanoprobe methods (STM, AFM, SNOM, ballistic electron energy microscopy)
- Submicron 2D and 3D optical imaging (classical, UV, confocal and scanning interference microscopy, laser scanning tomography)
- Spectroscopic techniques (PL & micro-PL, Raman & micro-Raman)
- Contactless electrical characterisation techniques
- Defect imaging using electrical transport characterisation techniques
- Electron beam methods (TEM, EBIC, CL)
- X-ray based techniques (topography, diffractometry, fluorescence)
- Defect mapping (of any type) over large area wafers
- Defect analysis in degraded optoelectronic and electronic devices
- Defects and degradation of organic semiconductors and devices
- Strategies for correlation of results from different techniques
- In-situ diagnostics and process control
- Specific sessions on defects in various classes of semiconductor materials with respect to their fields of application

Important Information

Early Registration Deadline:
15th August 2007

Conference Fees (before 15/08/07):

Participants	475 €
Students	375 €
Accompanying Person	350 €

Conference Fees (after 15/08/07):

Participants	525 €
Students	425 €
Accompanying Person	400 €

More information can be found on the conference website at:

http://www.drip12.de

What is DRIP?

The International Conference on Defects – Recognition, Imaging and Physics in Semiconductors (DRIP) is a conference on the physics of semiconductors with special emphasis on defects covering application aspects as well as fundamental questions regarding the physics of defects. The purpose of DRIP is to provide a forum for scientists / engineers from universities, research institutes and industry to meet and discuss the methods used for the recognition and imaging of defects in semiconductor materials and devices. The conference includes investigations of defects in raw materials (at the wafer level), process-induced defects, and defects that appear during operation of devices (burn-in, aging tests). DRIP has a history of more than 20 years with 11 successful conferences to date in Europe, Asia, and America. The field covered by DRIP can be described as "going from the extremely small to the extremely large". The main challenge of DRIP is to link defect images, transport/optical properties, and performance of actual devices.

WWW.BRIGHTER.EU at DRIP

Within the DRIP-XII conference there will be a special session “Defects in Devices” supported by the WWW.BRIGHTER.EU project. An invited talk will be given by Julien Nagle of Thales Research and Technology, France. Many other partners in the Consortium are also likely to contribute to this conference.

MBI Conference Chair
Dr. Jens W. Tomm
Max-Born-Institute
Email: drip12@mbi-berlin.de

MAX-BORN-INSTITUT

FBH Conference Chair
Dr. Ute Zeimer
Ferdinand-Braun-Institute
Email: drip12@fbh-berlin.de

Ferdinand-Braun-Institut für Höchstfrequenztechnik

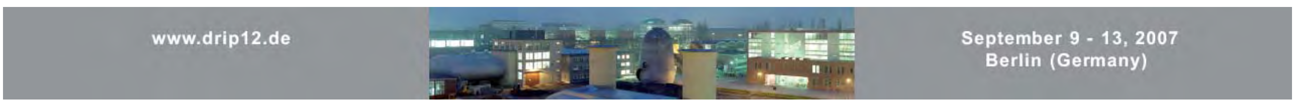

NUSOD CONFERENCE – SEPTEMBER 2007

7th International Conference on

Numerical Simulation of Optoelectronic Devices

24th – 28th September 2007, University of Delaware, United States

Conference Chairs: Joachim Piprek, NUSOD Institute and Dennis Prather, University of Delaware

The NUSOD conference connects theoretical research and practical device development in optoelectronics. Papers are solicited on the theory, modelling, simulation and analysis of optoelectronic devices including materials, fabrication and applications. Researchers, device engineers and software developers are invited to discuss the advancement and practical use of numerical tools in photonics and electronics. A Special Issue of Optical and Quantum Electronics will give NUSOD'07 authors the opportunity to publish expanded versions of their paper.

Find out more at:
www.nusod.org

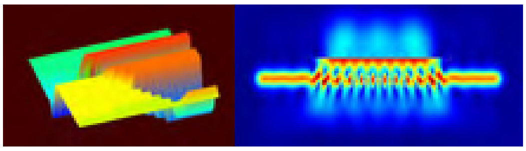

The **WWW.BRIGHTER.EU** Consortium is pleased to announce that three of its members are serving on the NUSOD '07 Program Committee:

- **Norbert Linder,** OSRAM Opto Semiconductor
- **Hans Wenzel,** Ferdinand-Braun Institute
- **Eric Larkins,** University of Nottingham

Prof. Larkins is also the primary guest editor of the Special Issue of Optical and Quantum Electronics.

CALENDAR OF EVENTS

The calendar below lists some events in the coming year at which the Consortium will be represented.

MAY 2007

6th – 11th
Conference on Lasers and Electro-Optics (CLEO)
Baltimore, Maryland, USA

JUNE 2007

9th – 16th
International Graduate Summer School on Biophotonics
Ven, Sweden

17th – 22nd
European Conference on Lasers and Electro-Optics (CLEO-Europe)
Munich, Germany

17th – 21st
European Conferences on Biomedical Optics (ECBO)
Munich, Germany

18th – 21st
LASER 2007 – World of Photonics Exhibition
Munich, Germany

SEPTEMBER 2007

9th – 13th
12th International Conference on Defects – Recognition, Imaging and Physics in Semiconductors (DRIP-XII)
Berlin, Germany

14th – 15th
European Semiconductor Laser Workshop (ESLW) 2007
Berlin, Germany

16th – 20th
33rd European Conference and Exhibition on Optical Communication (ECOC)
Berlin, Germany

24th – 28th
7th International Conference on Numerical Simulation of Optoelectronic Devices (NUSOD)
Newark, Delaware, United States

NOVEMBER 2007

14th – 17th
39th World Forum for Medicine – MEDICA
Düsseldorf, Germany

PARTNER PRESENTATIONS

In this section of the e-Newsletter, we introduce some of the partners in the project Consortium.

Each partner presentation provides an overview of the particular company / research institute / university, outlines their role within the project and provides details for the interested reader to obtain further information.

In this first edition of our e-Newsletter, profiles are presented for Rainbow Photonics AG and the Universities of Cambridge, Kassel and Nottingham. Over the course of the project, all partners will be covered in our planned series of six e-Newsletters.

Rainbow Photonics AG

Rainbow Photonics AG, is a Swiss company founded in Zürich as a spin-off of the Nonlinear Optics Laboratory at the Swiss Federal Institute of Technology (ETH) in 1997. Rainbow Photonics AG commercialises compact frequency-doubled blue lasers (BluePoint) operating at 430 nm and 488 nm, as well as all-solid-state infrared tuneable lasers.

The company also produces and commercialises optical components including waveguides, organic and inorganic crystals for photorefractive and electro-optic applications and Brillouin cells for optical phase conjugation. These products have been successfully introduced in the market. The fast developing field of optics and market situation requires dynamic growth in both research and development as well as in production.

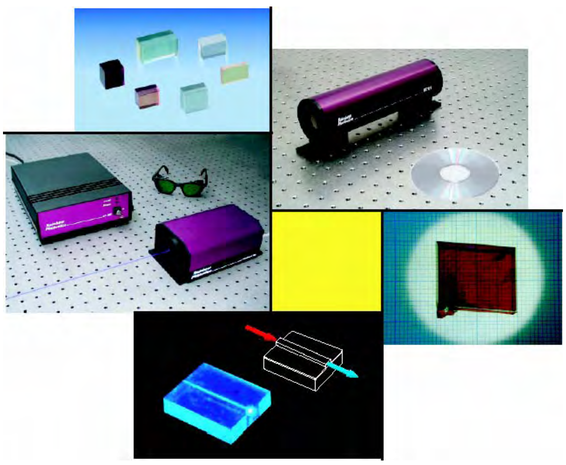

Rainbow Photonics products (clockwise from top right): Brillouin cells, DAST crystals, Waveguides for SHG, BluePoint lasers and various $KNbO_3$ crystals, pure and doped with different elements, for non-linear and photorefractive applications.

We have cooperation programs with many research groups, and with our continuous contact with customers and their ultimate needs, we can follow the direction where the market is going, and are able to react in advance to fast changes. We are present in all the major laser exhibitions worldwide and have representation offices overseas.

Carolina Medrano, CEO.

Activities within WWW.BRIGHTER.EU

Because of the experience in developing compact- all-solid-state frequency-doubled blue lasers, the role of Rainbow Photonics AG in the project is to bring their expertise to the realisation of a frequency-doubled ultraviolet laser for medical applications.

The objective within the frame of BRIGHTER is the development of pulsed compact, low-cost ultraviolet frequency-doubled lasers (340 nm) based on red external cavity laser diodes. In cooperation with RISOE and LLC, Rainbow Photonics will design and develop frequency-doubled lasers at 340 nm using a suitable SHG material.

In the final step a compact, pulsed prototype will be realised based on a single mode pump source of sufficiently high power at 680 nm developed by other partners within the project.

Further Information

Further information can be obtained from:

Dr. Carolina Medrano
Rainbow Photonics AG,
Technoparkstrasse 1,
CH-8005 Zürich,
Switzerland
Tel: +41 44 445 20 30
Fax: +41 44 445 20 31
Email: info@rainbowphotonics.com
Web: http://www.rainbowphotonics.com

University of Cambridge

The University of Cambridge is one of the oldest universities in the world and one of the largest in the United Kingdom. It has approximately 12,000 undergraduates and 6,000 postgraduate students and employs approximately 8,500 staff. It has a turnover of approximately 750M Euro, of which 300M Euro is spent on research. It is the centre of Europe's largest concentrations of start up activity – the so-called "Silicon Fen" – with over 1000 high-tech companies, generating approximately 3B Euro in revenues.

The Department of Engineering is the largest department in the University of Cambridge, representing approximately 10% of the University's activities by the majority of common metrics. It is one of Europe's largest integrated engineering departments, which includes approximately 1200 undergraduate and 500 PhD students.

Within the Department of Engineering, there is an active research activity in Photonics, with over 100 researchers working in the fields of soft materials, liquid crystals and photonic systems. The research group is housed in the new purpose-built Electrical Engineering Division building which provides custom office, laboratory and clean room space.

The new Electrical Division Building, opened April 2006.

The Photonics Systems Research activity has grown from approximately 15 people at its formation in the year 2000 to more than 40 people now. Results to date in Cambridge include the observation of spontaneous emission with anomalously high polarisation extinction in quantum dot laser diodes, the world's first mode-locked InGaAs quantum dot laser diodes leading to world-record repetition rates, pulse widths and jitter, the development of the world's first uncooled DWDM laser, the invention of a new form of variable gain, gain clamped SOAs, the demonstration of ultra-short (250 fs) pulses from laser diode based systems along with ultra-low jitter, and a new form of analogue to digital converter operating at 80 GSamples/s.

The group has successfully demonstrated practical RF links over MMF at carrier frequencies well beyond the fibre bandwidth (up to a world leading 20 GHz to date) and the development of 3G and WLAN Distributed Antenna System (DAS) networks, which are now being commercialised.

Particularly relevant to the BRIGHTER project is their work on high-power lasers incorporating integrated Fresnel lenses and the development of uncooled laser diodes with ultra-high linearity for RF signal distribution and also work on advanced modulation formats.

Activities within WWW.BRIGHTER.EU

Within the BRIGHTER project, the University of Cambridge is taking part in the following activities.

Fabrication of Novel Laser Structures

The Cambridge group was a pioneer in the modification of lasers using focussed ion beam etching, successfully developing integrated Fresnel lenses for enhancing laser brightness within the BRIGHT project. Within the BRIGHTER project, Cambridge will develop beam steering and gain levering lasers via contact separation.

High-Power Dynamic Laser Simulations

Cambridge will develop their dynamic laser model to study coupled laser arrays and further adapt it so that it can study the high bandwidth modulation properties of tapered high-power laser structures.

Optical Wireless Applications

Cambridge will develop optical wireless systems using the high-power lasers being developed by other partners within BRIGHTER. Here advanced modulation schemes, designed to overcome the effects of turbulence, will be studied and line-of-sight links between buildings will be demonstrated.

Display Applications

Cambridge will provide specifications and feedback on the performance requirements of high-power visible lasers for display applications. They will also provide a test bed where the visible lasers can be tested as part of a holographic projection display demonstrator.

Further Information

Further information can be obtained from:

Prof. Richard Penty
Tel: +44 1223 748358
Email: rvp11@cam.ac.uk
Web: http://www-g.eng.cam.ac.uk/photonic_comms

University of Kassel

The group at University of Kassel is within the Institute of Nanostructure Technologies and Analytics (INA), originally founded in 1997 as the Institute of Microstructure Technologies and Analytics (IMA) and renamed in 2005. The institute is a joint laboratory between the physics and electrical engineering departments. The groups within the institute are investigating new micro- and nano-fabrication techniques, device structures and concepts based on III-V and Si technologies. The institute has about 400m^2 of clean rooms (class 1000 to class 1) and another 400m^2 of laboratory space with an extensive infrastructure, which includes three MBE systems for III-V materials, patterning by optical and e-beam lithography, semiconductor processing (etching, deposition, evaporation) and a range of characterisation tools (AFM, STM, SEM, X-Ray, ellipsometry, etc.).

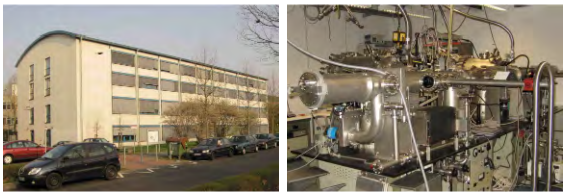

Institute of Nanostructure Technologies & Analytics (INA) at Kassel (left), 2-chamber MBE system at INA (right).

Within the INA, the technological physics group has been headed by Johann Peter Reithmaier since 2005. Previously he worked at the University of Würzburg, where he was responsible for a research group investigating new nanostructure technologies and optoelectronic device concepts. During this time, the research group developed quantum dot (QD) laser materials and devices for different wavelength ranges (1.0, 1.3, 1.5-2.0 µm). By tailoring the gain function with the dot dimensions, the group were able, for the first time, to stabilise the emission wavelength of QD lasers, making coolerless high-power pump modules for fibre amplifiers and lasers a possibility. The former group at Würzburg also realised ultra-short edge-emitting QD lasers with deeply etched Bragg mirrors (world record of 12 µm long lasers and 1 mA threshold current with 1 mW cw output power for a 30 µm cavity length). The group also achieved a record high direct modulation bandwidth of 37 GHz for InP-based 1.5 µm lasers by introducing the concept of a “coupled cavity injection grating”, which utilises coupling into higher order photonic cavity resonances and improves the limitations caused by the electron-photon coupling by factor of more than 4. Focused ion beam technologies were used to develop highly reliable grating fabrication methods, which allow maskless patterning of 1st order gratings for InP-based DFB lasers.

The new group in Kassel is continuing the activities on QD material development based on the self-organization of III-V QDs. The work is being extended to new fabrication technologies, which combine the high resolution and positioning control of state-of-the-art electron beam patterning with defect-free growth techniques to overcome current restrictions in the geometry control of nano-structures. A major interest is also looking to utilise this new class of material in device applications, (single photon sources, high-speed optoelectronic devices and high-power lasers). For this approach, one MBE system is dedicated to GaAs and one to InP-based materials, allowing wavelength coverage from the visible down to the near infrared.

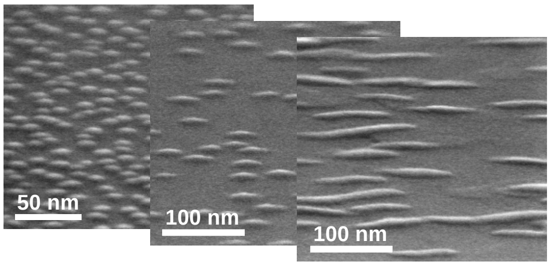

SEM images of uncovered QDs with different geometries as controlled by the growth parameters.

The former group in Würzburg was active in several EC projects (BIGBAND, NANOPT, NANOLASE, ULTRABRIGHT, WWW.BRIGHT.EU). Currently the group in Kassel is involved in four European projects (Pronano, QPhoton, Tasnano, WWW.BRIGHTER.EU).

Activities within WWW.BRIGHTER.EU

Within the project, the University of Kassel is realising QD laser structures at 920 nm with tailored QD geometries for coolerless pump laser applications as well as 920 nm and 1060 nm high-performance next generation QD laser material optimised for high wall-plug efficiency, high temperature stability and ultra-low alpha factors for high-brightness tapered lasers with an improved filamentation threshold. The aim of this approach is to explore the possibility of overcoming single mode output power limitations of conventional QW based technologies by using nanostructured laser material. While the 920 nm laser material will be used for pumping fibre lasers, the 1060 nm material is for devices that will be frequency-doubled to achieve green lasers for display applications.

Further Information

Further information can be obtained from:

Prof. Johann Peter Reithmaier

Tel: +49 561 804 4430

Email: jpreith@physik.uni-kassel.de

Web: http://www.ina.uni-kassel.de

University of Nottingham

The Photonic and Radio Frequency Engineering Group (PRFEG) in the School of Electrical and Electronic Engineering pursues cutting edge research in photonics and microwave technology. PRFEG researchers have come from a wide range of cultural backgrounds to create a dynamic and enthusiastic research environment. The group's activities are organised along three strands, funded by the EC, EPSRC and industry.

The activities of the High-Power Optoelectronics research strand, established 12 years ago, have contributed to the European high-power laser projects WWW.BRIGHT.EU, ULTRABRIGHT, POWERPACK and NODELASE. The strand's activities focus on: a) the design and modelling of high-power and high-brightness lasers; b) reliability and degradation studies of laser diodes; and c) the development of novel high-brightness laser diodes. The Group has successfully developed 2.5D & 3D coupled models (i.e. optical, electronic & thermal), including a multi-wavelength model for the predictive design and simulation of laser diodes. Advanced models for gain dynamics and thermal effects in laser diodes have also been developed. Over a number of years, we have developed a flexible, state-of-the-art facility for characterising optoelectronic materials and devices (OMES).

PRFEG's OMES characterisation laboratory.

The activities of the Photonic Communications Technology research strand are focused on studying devices, physical effects and materials that will, over the next decade, have a major impact on communications infrastructure. These include gain dynamics and non-linear optical effects in SOAs for wavelength conversion and functional photonics, novel optical materials and optical power budget/amplification in photonic integrated circuits. A particular emphasis is given to optical sampling using SOA-based four wave mixing for pulse characterisation and BER estimation. A further activity is looking at the non-linear effects of components in optical network / system contexts including transmission of rf signals over fibre.

The RF Devices, Circuits and Materials research strand activities grew out of a close interaction with the School of Physics. The activities are more oriented towards the interaction of microwaves with materials in general as well as the design of microwave integrated circuits for material assessment applications. In collaboration with the applied optics group, we are investigating active pixel circuits operating above 1 GHz. Devices for microwave power and millimetre waves are being actively investigated. The strand is benefiting from the purchase of a new vector network analyser that will allow the characterization of active and passive rf devices and circuits to 330 GHz.

PRFEG belongs to the University of Nottingham Institute of Materials (UNIMAT) and plays a leading role in the UNIMAT Interdisciplinary Doctoral Training Centre (IDTC) for Photonics and Electronics, which is funded by the University to stimulate interdisciplinary research and training between the Schools of Electrical and Electronic Engineering, Physics, Chemistry and Mechanical, Materials & Manufacturing Engineering.

Activities within WWW.BRIGHTER.EU

Within the project, the University of Nottingham (UNott) is contributing in the areas of laser diode simulation and design, advanced characterisation and reliability studies.

UNott is further developing their spectral laser simulation tool to include the capability to simulate high-brightness external cavity laser diodes and phase-coupled mini arrays. UNott is also working on the simulation and design optimisation of tapered lasers with split contacts at 1060 nm for display applications.

UNott will perform intracavity electroluminescence imaging measurements on tapered lasers, which will be used for advanced validation of the spectral laser simulation tool. UNott is also using the by-emitter degradation analysis method to look at bar-level degradation processes due to thermal, electrical and mechanical interactions between emitters in both red-emitting laser bars and laser bars mounted on different heatsink technologies. The existence of near- and mid-infrared defects in near-infrared laser diodes will be investigated by the Max-Born-Institute and UNott.

Finally, UNott are responsible for co-ordinating the WWW.BRIGHTER.EU training, dissemination and popularisation activities.

Further Information

Further information can be obtained from:

Prof. Eric Larkins
Tel: +44 115 951 5534
Email: eric.larkins@nottingham.ac.uk
Web: http://hermes.eee.nott.ac.uk/prfeg

Review on Short Range Optical Wireless Communication Systems

C. H. Kwok, Richard V. Penty and Ian H. White

Centre for Photonic Systems, Centre for Advanced Photonics and Electronics, Department of Engineering, University of Cambridge, 9 J J Thomson Avenue, Cambridge, CB3 0FA, U.K.

Introduction

Optical Wireless (OW) refers to the transmission of modulated visible or IR beams to obtain broadband communications. Like fibre systems, OW uses lasers to transmit data, but instead of transmitting the signal over fibre, it sends it through the air. Commercially available OW systems typically offer capacities in the range of 100 Mbps to 2.5 Gbps. These systems are compatible with a wide range of applications and markets, and they are sufficiently flexible as to be easily deployed.

OW provides an attractive solution to the last-mile problem, especially in densely populated urban areas. These short range regional networks require moderate bandwidth but high flexibility in deployment. From the technical point of view, deployment of these networks can be provided on demand without the extensive prior construction of an expensive infrastructure as in the case of fibre-based optical networks. The license free operating wavelength bands also ease the deployment of such OW transmission links. Figure 1 illustrates the idea of intra-building networking through OW.

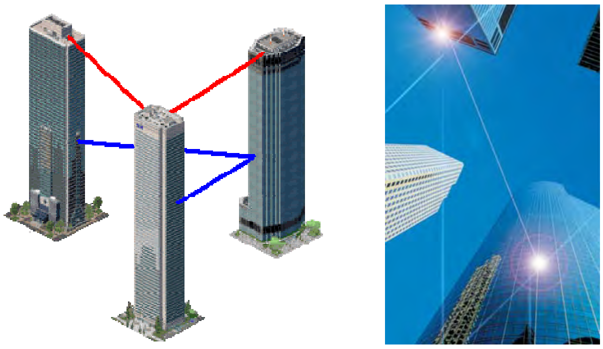

Figure 1: Schematic illustration of an intra-building optical wireless network.

OW can be categorised into indoor and outdoor scenarios. In this tutorial, we will focus on the short range outdoor OW systems for high data rate intra-building networking applications. Optical transceivers in such outdoor transmission links can be installed in the windows, or more typically on the rooftops, of buildings, and communicate with regional network nodes to bypass the local optical fibre networks which may not be available or accessible to network subscribers. The performance of OW systems, however, suffers inevitably from atmospheric conditions in the surrounding environment. Hence, the distance between the OW transceivers should generally be kept short (normally <500 m) to ensure the reliability of the optical connection between subscribers and/or network nodes. This short distance wireless connection can generally be achieved in most of the cases for cities with a high population density and many high-rise apartments.

Transmission over the atmosphere suffers from both attenuation and turbulence effects.

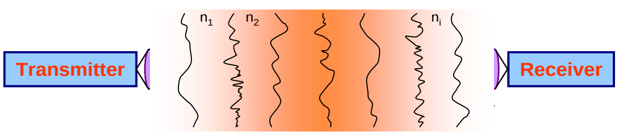

Figure 2: Atmospheric turbulence channel typically faced in optical wireless systems.

The atmospheric attenuations limit the distance an OW signal can transmit given a power budget in the power-starved OW systems, while the atmospheric turbulence as illustrated in Fig. 2 introduces both intensity and phase fluctuations for the received signal.

Hence, typical simple intensity modulation with direct detection (IM/DD) schemes are currently preferred over advanced phase or frequency modulation schemes in OW systems, in part because of the distortion introduced by turbulence.

In this tutorial, we review system considerations for an OW system and list applications and research directions.

Link Configurations

There are two basic configurations of the OW communication channel: direct line-of-sight (LOS) and diffuse paths between transceivers. Figure 3 shows schematic illustrations of these two types of link configuration.

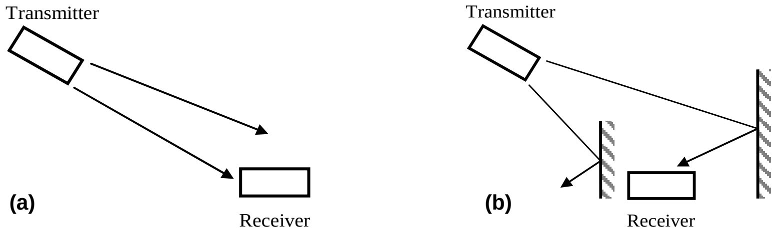

Figure 3: Schematic illustration of (a) direct line-of-sight and (b) diffuse path OW link configurations.

Direct LOS systems transmit the signal directly between a LOS transmitter and receiver. They can either be a system with a narrow transmitting beam dedicated for a single receiver, or a diverged beam to provide certain coverage where multiple receivers could be possible. The trade-off between the coverage and the overall path loss governs the mobility/reliability of the receiver(s) and the maximum data rate of the transmission link. In a narrow beam system, the channel bandwidth is maximised but mobility is restricted and beam tracking is usually required to avoid misalignment between transceivers due to mechanical perturbations and to ensure the link reliability. The use of a diverged beam to improve the signal coverage, however, introduces excess loss to the overall path, which is not favourable in power-starved OW systems.

In a diffuse system a diverging data modulated light source illuminates the coverage space, and a receiver within the coverage space detects this free space transmitted signal. Diffuse systems are robust to blocking and do not require precise alignment between transceivers, as many paths exist from the transmitter to the receiver. However, the path loss of such systems is high and inter-symbol-interference is introduced by multi-path signal reflections before entering the receiver.

Transmitters

Depending on the application, the link configuration and the transmission range, either light emitting diodes or lasers are used as the light source in OW systems. In the near-IR region (between the visible and 1400 nm) the safe power limit for point sources is less than 1 mW. Beyond 1400 nm, this limit increases by a factor of 20. This difference is due to the different spot size of a collimated beam focused onto the retina and to the sensitivity of the retina to damage at different wavelengths. Table 1 lists the classes of laser output power limit at different wavelengths. Much higher powers are available at any wavelength by diffusing the sources, thus increasing their apparent emitted areas.

Indoor applications of the OW systems must comply strictly with the eye safety conditions, while outdoor systems considered here generally use high-power lasers that operate above this power constraint to achieve a good power budget. The safety standard recommends that these high-power systems should be located where the beam cannot be interrupted or viewed inadvertently by a person. Rooftop locations or high walls are usual for this type of system.

Class	650 nm (visible)	880 nm (infrared)	1310 nm (infrared)	1550 nm (infrared)
1	< 0.2 mW	< 0.5 mW	< 8.8 mW	<10 mW
2	0.2 to 1 mW	N/A	N/A	N/A
3A	1 to 5 mW	0.5 to 2.5 mW	8.8 to 45 mW	10 to 50 mW
3B	5 to 500 mW	2.5 to 500 mW	45 to 500 mW	50 to 500 mW
4	> 500 mW	> 500 mW	> 500 mW	> 500 mW

Table 1: Laser safety classifications for a point-source emitter (note that Class 2 only applies to visible light sources).

Regardless of the type of light source, direct modulation is generally applied to simplify the transmitter design and minimise the cost.

Transmission Wavelength

Absorption of light in the atmosphere is caused by the atmospheric molecules, such as carbon-monoxide molecules, water droplets and oxygen molecules, which have high absorption in the infrared band. The wavelength dependent characteristics of this absorption are essentially the same as that present in optical fibres with low-loss transmission windows at certain infrared bands. However, different environmental conditions display very different wavelength-dependant transmission characteristics, and hence there is no preferred wavelength for OW communication systems. Although there is no dominant wavelength in OW communication systems, wavelengths in the infrared region are commonly used for high data rate (> Mb/s) transmission to take advantage of the well-developed devices from the existing optical communications field.

Modulation Schemes

The robustness of the IM/DD scheme to the incoherent fluctuation of atmospheric turbulence makes it suitable for OW systems, as coherent communication schemes are difficult to implement because of phase front distortion by the atmospheric turbulence. This phase distortion makes the matching of an incoming beam to the phase front of a local oscillator difficult. In contrast IM is suitable for dealing with the incoherent fluctuation of atmospheric turbulence by simply counting the number of photons received in detecting the digital signal.

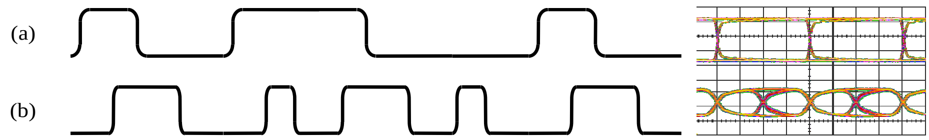

Figure 4: Schematic illustration of (a) NRZ-ASK and (b) Manchester coded NRZ-ASK of a bit pattern '10110010' shown with the corresponding experimentally measured eye diagrams.

Besides the simple typical non-return-to-zero (NRZ) amplitude-shifted keying (ASK) modulation schemes, Manchester coded ASK is also a common signalling scheme for OW owing to its unique feature in signal detection. In a Manchester coded ASK signal, the binary bit-*0* and bit-*1* are represented with the same pulse at different positions within a bit slot. Although this coding scheme requires twice the bandwidth of its data rate, it has advantages for OW communication to combat the slowly varying channel fading as dispersion-induced pulse spreading is no longer an issue in free space transmission. Detection of the received Manchester signal is done through a half-bit-delayed differential decoder, to generate a symmetric output signal with zero dc-component. A constant decision threshold set at zero is optimal for the detection of a decoded Manchester signal regardless of the turbulence-induced fading because of the symmetry of the decoded signal along the zero level. The same situation cannot be applied to NRZ schemes, as the turbulence-induced fading introduces a power fluctuation to bit-*1* (on-state) but not bit-*0* (off-state), causing an asymmetrical noise profile between the two states.

Receivers

An OW receiver consists of several main sub-systems: an optical system to concentrate and collect incoming light to a photodetector which converts the optical signal back to the electrical domain; an optical filter which rejects the background ambient noise; and an optical pre-amplifier which improves the receiver sensitivity.

The light collecting element can make use of either imaging or non-imaging optics to condense a spatially spread signal beam and focus it onto the light detecting element. Here, a photodetector with a sufficiently large active area is needed to provide a large field-of-view for the receiver and high conversion efficiency between the received optical power and the detected electrical signal. Such a large active area photodetector, however, has a very high capacitance which leads to a limitation for high data rate operation. The bandwidth of the photodetector can be improved by reducing the size of this active area. However, a small area photodetector incurs a greater coupling loss due to the small aperture they present to the incoming beam, so a careful trade-off between these factors is necessary to optimise the final performance. The out-of-band background ambient noise can be rejected by optical filtering to prevent its intensity from saturating the photodetector. The receiver sensitivity can be improved through optical pre-amplification by amplifying the received optical signal before detection to minimise the thermal and shot noise of the photodetector. In case of narrow beam systems, active beam tracking is also needed to maintain the LOS condition for transmitter and/or receiver vibrations.

Atmospheric Channel

OW communications are subject to various kinds of path loss. The power budget of an OW system is strongly determined by atmospheric loss along the propagation path. A free space transmitted signal is attenuated by absorption and scattering with water droplets and gases. Depending on the size of these molecules or particles, light may be absorbed as a power loss, or scattered with the propagation direction deviated from its original path.

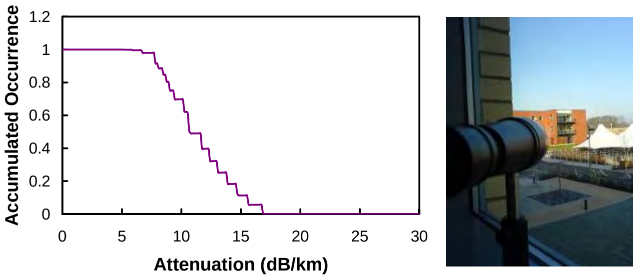

Figure 5: Accumulated occurrence of the atmospheric attenuation in the Cambridge, UK region for a 2-year period. The photograph shows the setup at the Centre for Advanced Photonics and Electronics (CAPE) Building for the receiver telescope pointing towards the William Gates Building.

In either case, these particles prohibit the light from reaching the receiver and optical loss is incurred along the transmission link. Furthermore, diverged and diffused systems have an additional considerable power loss related to the beam divergence. Figure 5 plots the cumulative distribution of the free space transmission loss in the Cambridge, UK region using local weather information. The plot considers all the possible sources of atmospheric attenuation such as rain, fog and snow, and illustrates how atmospheric attenuation plays a dominant role in limiting the transmission range under a severely attenuated free space channel.

Even in clear weather conditions, the atmosphere along the transmission link is not completely benign and its condition varies slowly. This slow variation of the atmospheric conditions will lead to inhomogeneities in temperature and pressure of the atmosphere causing refractive index variations along the transmission link. Hence, a slowly varying signal fading is the result in a free space transmitted signal. Solutions to this slowly varying signal fading include the use of advanced signalling schemes (e.g. Manchester coding), adaptive power equalisation and signal diversity reception.

Applications of OW Systems

There are several areas where OW is attractive over its radio frequency (RF) counterpart. Such applications include secure wireless communications, ultra-high bandwidth short range wireless communication, wireless communication in radio hazardous areas etc. Owing to the unique feature of dedicated transceiver alignment, the signal can be securely transmitted by a narrow beam LOS OW transmission link whose signal cannot be tapped without interfering with the transmission. The unregulated wavelength band allows virtually unlimited bandwidth for indoor and outdoor short range high bandwidth wireless signal transmission which is otherwise not achievable with RF technology. Perhaps the major application of the OW systems is in the areas where RF cannot be used such as hospitals and airports. Furthermore, networking between buildings which may be protected from construction of any new infrastructure (e.g. historical buildings) can only be implemented with wireless technology.

Summary

We have reviewed the principal developments if the field of OW. It is clear that OW may find applications in high data rate short range transmission links. While this technology is approaching a good degree of maturity, comprehensive performance analysis on enhancing system reliability and flexibility for short range OW systems is a clear current research direction in this area. Development of new generation of lasers with sufficiently high power and modulation bandwidth will allow a more compact the transmitter design and enhance the transmission performance for outdoor applications.

Advanced modulation and link availability assurance schemes are also the focus of much current research in OW systems to improve the robustness of transmitting signals over free space.

Reference Information

- http://www.fsona.com
- http://www.cablefreesolutions.com
- The Met Office, FitzRoy Road, Exeter, Devon, U.K.

Technology and Applications of Frequency-Doubled High-Brightness Laser Diodes

Carolina Medrano

Rainbow Photonics AG, Technoparkstrasse 1, CH-8005 Zürich, Switzerland

Introduction

The first experiment on frequency doubling of laser diodes was published in 1979 in a collaborative effort between ETH and North American Philips [1]. The doubling element was potassium niobate ($KNbO_3$) grown at ETH-Zürich. In order to achieve large fundamental output powers, the laser source was operated in a pulsed mode at high drive current levels.

This was the beginning of blue light generation by nonlinear optical interactions, such as second-harmonic generation (SHG) and sum-frequency generation (SFG) with diode lasers [2] (e.g. AlGaAs and InGaAs) and diode-pumped solid-state lasers (e.g. Nd:YAG and Cr:LiSAF). Now it is an attractive approach to realise compact all-solid-state blue lasers and research in this topic has continued in different institutions worldwide, including ETH-Zürich. This exciting topic was followed by doubling experiments performed in waveguides [3] implanted in $KNbO_3$.

Figure 1: "BluePoint" Commercial blue laser system from Rainbow Photonics AG.

Frequency up-conversion of near infrared laser diodes offers the potential of robust and reliable blue laser sources. With better laser diodes now being offered commercially, it has been possible to demonstrate a compact continuous-wave blue-green laser by direct frequency doubling a monolithically integrated master-oscillator power-amplifier (MOPA) laser diode in a 17 mm long $KNbO_3$ crystal [4]. With a successful technology transfer from ETH-Zürich to Rainbow Photonics, the first all-solid-state blue lasers operating at 430 nm and 488 nm were offered commercially in 1998 (see Fig. 1). These lasers have had a large impact in the biomedical area and also in confocal microscopy. The development of frequency-doubled lasers has continued due to their technological advantages over existing bulky and expensive sources. In addition, other applications are now being targeted such as health-care, environment, security, cancer diagnosis and therapy.

Lasers for Application in the UV

Laser diodes have experienced great advances and offer an amazing compactness at a reasonable cost. However, their performance still needs some improvement to satisfy both existing and emerging markets. In addition for some special applications in the medical area particular wavelengths are required that are not presently available from reliable laser diodes, and the only currently available sources are bulky and expensive.

For photodynamic therapy and laser induced fluorescence applications, light sources operating at ~ 405 nm, are needed. Within the framework of the WWW.BRIGHT.EU project (IST–511722), frequency-doubling of high-power, single-frequency laser diode systems operating at 810 nm were proposed. External cavity tapered laser diodes operating at 810 nm were also developed during the project. The nonlinear material selected was periodically-poled KTP and various configurations were proposed and tested. Using a bow-tie cavity configuration, a compact prototype was realised obtaining a record of 220 mW of blue light at 405 nm in an almost diffraction-limit beam [5].

All-solid-state ultraviolet lasers operating in the wavelength range of 200 nm to 350 nm are extremely attractive for biomedical applications, fluorescence diagnostics, microlithography and optical data storage. The light source needed for fluorescence diagnostics that will be developed within WWW.BRIGHTER.EU must operate at 340 nm in a pulsed regime with several mW of output power. The final system must be reliable, cost efficient and also allow a real time monitoring system to be developed. A second harmonic generation approach based on red laser diodes will be implemented. Other partners in the consortium will develop high-brightness laser diodes operating at 680 nm for this purpose.

UV Lasers Operating at 340 nm

Ultraviolet diode lasers emitting below 350 nm are extremely difficult to produce. Therefore a realistic approach to build all-solid-state lasers operating at this wavelength is to use optical frequency conversion of visible lasers in a nonlinear crystal that is transparent in the UV.

In Table 1 we list the different borate crystals that are suitable for frequency doubling into 340 nm according to their transparency range. QPM Mg:$LiNbO_3$ is also a candidate from the point of view of its transparency range, which starts at 305 nm. However, the damage threshold of 10 MW/cm^2, although higher than that in $LiNbO_3$, and the stability of the material makes the use of it in devices for our application questionable. All these borate crystals have a relatively high nonlinearity (1-3 pm/V). In BBO the nonlinearity is higher (d_{22} = 2.3 pm/V) and the damage threshold is very high (> 5 GW/cm^2 @ 532 nm).

Borates	Transparency Range (nm)
β-BaB_2O_4 (BBO)	190-3000
BiB_3O_6 (BIBO)	286-2500
LiB_3O_5(LBO)	155-3200

Table 1: Nonlinear crystals for second harmonic generation into UV.

In a first approach the selected material for second harmonic generation into 340 nm is BBO. The final device should have the following specifications: a) Peak power > 200 mW to 400 mW, b) Pulsed regime operation: 100 ns, 5 kHz – 10 kHz, c) $M^2 < 1.2$ for efficient fibre coupling. The pump sources will be developed by other partners in the project and consist of tapered diodes with output powers of up to 3-4 W at 680 nm and $M^2 < 1.2$.

Recently the generation of continuous-wave ultraviolet laser light at λ = 278 nm by optical frequency doubling of visible light in BBO-waveguides has been reported [6]. High conversion efficiencies have been demonstrated using bulk BBO in resonant cavities with high power lasers [7]. This approach requires an active stabilisation of the cavity length and a single frequency pump laser. The research activities in the first phase of the WWW.BRIGHTER.EU project will test and evaluate both approaches i.e. generation of UV light at 340 nm using both bulk crystals and waveguides. The final laser system must be reliable, user friendly and cost efficient.

References

[1] P. Günter, P.M. Asbeck and S.K. Kurtz, "Second-harmonic generation with $Ga_{1-x}Al_xAs$ lasers and $KNbO_3$ crystals" *Appl. Phys. Lett.*, **35,** 461-463 (1979).

[2] D. Fluck and P. Günter, "Tunable blue light generation by sum frequency mixing of AlGaAs and InGaAs laser Diodes in $KNbO_3$" *Electron. Lett.*, **32,** 901-903 (1996).

[3] T. Pliska, D. Fluck, P. Günter, L. Beckers and Ch. Buchal, "Linear and nonlinear optical properties of $KNbO_3$ ridge waveguides" *J. Appl. Phys.*, **84,** 1186-1195 (1998).

[4] D. Fluck and P. Günter, "Efficient generation of CW blue light by sum-frequency mixing of laser diodes in $KNbO_3$" *Opt. Commun.*, **136,** 257-260 (1997).

[5] WWW.BRIGHT.EU "*Wide Wavelength Light for Public Welfare: High-Brightness Laser Diode Systems for Health, Telecom and Environment Use*" EC Contract No. IST-511722, see http://www.bright-eu.org.

[6] R. Degl'Innocenti, A. Guarino, G. Poberaj and P. Günter, "Second harmonic generation of continuous wave UV light and production of β-BaB_2O_4 optical waveguides" *Appl. Phys. Lett.*, **89,** 041103 (2006).

[7] K. Kondo, M. Oka, H. Wada, T. Fukui, N. Umezu, K. Tatsuki and S. Kubota, "Demonstration of long-term reliability of a 266nm CW quadrupled laser using β-BaB_2O_4" *Opt. Lett.*, **23,** 195-197 (1998).

High-Power High-Brightness Lasers

M.T. Kelemen, J. Weber, G. Kaufel, R. Moritz, M. Mikulla and G. Weimann

Fraunhofer Institute for Applied Solid State Physics, Tullastr. 72, D-79108 Freiburg, Germany

Introduction

High-power, high-brightness diode lasers are gaining more and more interest for applications previously dominated by expensive and inefficient solid-state lasers due to their better efficiency, brightness and compactness. The significant fact about conventional high-brightness optical sources is that they exhibit about an order of magnitude higher brightness than broad-area semiconductor lasers. For a tapered diode laser the brightness is defined approximately to [1]

$$B = \frac{P}{\lambda_0^2 M_\perp^2 M_=^2} \qquad (1)$$

where λ_0 is the vacuum wavelength and M^2 the beam propagation parameter perpendicular to and in the plane of the epitaxial layer.

Today broad-area diode lasers are used to achieve high output powers. However, standard broad-area waveguide designs are susceptible to modal instabilities, filamentation and catastrophic optical mirror damage (COMD) [2]. This results in low beam qualities and values for the brightness limited to around 1×10^7 $Wcm^{-2}sr^{-1}$. On the other hand, high beam qualities are realised with ridge lasers emitting in a diffraction-limited optical beam. The reliable output power of these lasers is mainly limited by the onset of facet degradation, which depends on the power density on the facet. Due to the small stripe width of a few microns, the output power is typically limited to several hundreds of milliwatts resulting in a brightness of less than 1×10^8 $Wcm^{-2}sr^{-1}$ [3].

A lot of different solutions have been proposed in the last few years to overcome these problems and to achieve high output power together with high beam quality. The main effort has been directed to develop broad-area structures that support only one lateral mode. Tapered devices [4,5], distributed feedback (DFB) lasers [6,7] and monolithically integrated Master-Oscillator Power-Amplifiers (MOPAs) [8] have been demonstrated and all of them are able to produce output powers well above 1 W together with a high beam quality.

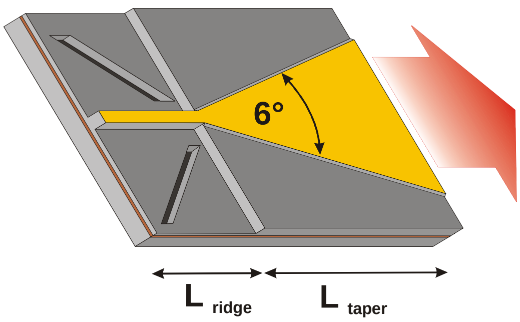

Figure 1: A tapered diode laser with a ridge waveguide for mode filtering.

Among these, devices based on laterally tapered gain sections in combination with ridge-waveguide sections as depicted in Fig. 1 seem to be the most promising candidates when a reproducible and low cost fabrication is a further requirement. For the other concepts a costly epitaxial re-growth step or the fabrication of a holographically defined reflection grating is necessary, lowering the manufacturing yield. Tapered diode lasers produce diffraction-limited output powers up to several Watts in continuous wave operation. The value of the brightness for a 1 W laser emitting a diffraction-limited beam at 1 µm wavelength is 10^8 $Wcm^{-2}sr^{-1}$ according to equation (1). Hence tapered diode lasers provide a brightness of up to a few times 10^8 $Wcm^{-2}sr^{-1}$ in comparison to a few times 10^7 $Wcm^{-2}sr^{-1}$ for conventional semiconductor lasers.

This article is focused on the design and performance of high-power diode lasers comprising ridge and tapered sections for near diffraction-limited output power in the multi-watt regime optimised for the GaAs-based wavelength of 975 nm. It gives an overview of experimental work that has been carried out in order to improve the beam quality as well as to enhance the output power of these devices.

Fabrication of Tapered Devices

The fabrication of high-brightness lasers with high conversion efficiencies requires an epitaxial layer sequence with low internal losses (< 2 cm^{-1}), low confinement factor (<1.5 %) and high internal conversion efficiency (> 90%). The reduction of the internal losses and of the confinement factor can be achieved by broadening the waveguide layers [9]. This reduces the overlap of the optical mode with the highly doped cladding layers.

The active region consists of a single InGaAs quantum well embedded in a 1.06 µm thick AlGaAs core region with 20% Al content. The use of high bandgap (E_g = 1.68 eV) AlGaAs core layers with 20% Al leads to a strong carrier confinement. The quantum well is 7 nm thick with a nominal In content of 19% resulting in an emitting wavelength of 976 nm. The optical waveguide is formed by 1 µm thick AlGaAs claddings with 40% Al. Si and Be have been used for n- and p-type doping, respectively. The layer design exhibits an overlap of the fundamental optical mode with the quantum well of 1.1% for 976 nm. It has been shown previously that this low modal gain epitaxial layer structure suppresses beam filamentation in tapered lasers [10].

For a pre-characterisation of internal parameters, broad-area lasers are obtained from a fast process. The p-side metal is deposited by using a shadow mask, and the n-side contact is applied to the unthinned substrate. Laser bars with as-cleaved facets are mounted p-side up for pulsed characterisation. The high material quality of the MBE-grown laser structures yields a high internal efficiency of more than 97%. Low internal losses of less than 0.5 cm^{-1} are obtained from Fabry-Perot laser diodes of different lengths.

The ridge and taper sections are processed by using optical lithography and wet chemical etching followed by a lift-off step. Figure 1 shows a schematic of the device. The structure consists of a taper angle of 6° together with a taper section length typically between 2 and 3 mm. The length of the ridge section can be varied between 100 and 1000 µm. The ridge height is chosen appropriately for the propagating wave to fill the taper angle. Cavity-spoiling groves on both sides of the ridge section suppress undesired Fabry-Perot modes.

After thinning and cleaving, a highly reflective double-stack of Si and SiO_2 (95 % reflectivity) is deposited on the back facet by reactive magnetron sputtering. Two different anti-reflection coatings are used for the front-facet: (i) a single layer of SiN (<1 % reflectivity) and (ii) a single layer of SiON (<0.01 % reflectivity). In principle this device can function as either an amplifier [4,10] or as a laser depending on the rear facet coating. Finally the devices are mounted p-side down on copper mounts with indium solder. Uniform pumping of the laser medium is achieved by current injection via bond wires.

Theoretical Background

Causes of Filamentation Processes

In broad-area devices, beam filamentation is the main physical effect that limits the device performance when high beam quality is required. With increasing power levels, spatial hole burning occurs due to the interaction between the amplified optical field and the carrier density in the active region. Therefore, the complex optical index becomes inhomogeneous and leads to self-focusing of the optical wave. This results in filament formation which severely deteriorates the beam quality [11]. The dependence of the complex optical index n on the carrier density n_c of the active layer is given by [12]:

$$n(n_C) = n_0 - \frac{1}{2k_0} g_m(n_C)\cdot\alpha_H + \frac{i}{2k_0}\left[g_m(n_C) - \alpha_i\right] \tag{2}$$

In this equation, $g_m(n_c) = \Gamma g(n_c)$ is the modal optical gain given by the product of the material gain $g(n_c)$ and the optical confinement factor Γ. The optical confinement factor is determined by the overlap between the vertical mode profile in the waveguide structure and the active layer. α_H is the linewidth enhancement factor, k_0 the vacuum wavenumber, n_0 the carrier independent part of the optical index, and α_{opt} are the total optical losses, respectively. In order to achieve lateral coherence and to suppress filament formation in semiconductor lasers to reach high brightness, three principles are crucial:

- The differential optical index $\partial \bar{n}_{eff}(n_C)$ is proportional to the linewidth enhancement factor α_H. Therefore by finding ways to lower α_H it is possible to reduce the sensitivity against self-focusing and filamentation (e.g. diode lasers based on quantum dot structures have shown to posses an inherently low linewidth enhancement factor).

- Minimising the optical losses α_{opt}, especially the resonator and geometrical losses.
- As has been theoretically and experimentally analysed in [10,13], the differential optical index is proportional to the confinement factor squared. So a reduced confinement factor also reduces the variation of the optical index due to spatial-hole burning.

Within this work the last point has been actually realised through epitaxial design. In this work we have varied the length of the tapered section and therefore we have changed the optical losses systematically. In the case of a tapered diode laser the optical losses consist of the internal optical losses α_i, the resonator losses α_R and additionally a geometrical part (as additional resonator losses) due to the tapered resonator design, which are well described by [12]:

$$\alpha_{opt} = \alpha_i + \alpha_R - \frac{1}{2(L_1 + L_2)} \ln\left(\frac{W_1^2 n_{eff}}{4\lambda L_2}\right) \tag{3}$$

In general (α_i = constant) the different parts of the optical losses become smaller with longer taper lengths.

Astigmatism and Corrected Farfield

In order to determine whether the beam quality is diffraction limited, the measurement of interest is not the angular width of the output beam (far-field) as normally used for broad-area diode lasers, but rather a measurement that is more sensitive to beam quality, a measurement of the beam at a waist called "corrected far-field" [1,4].

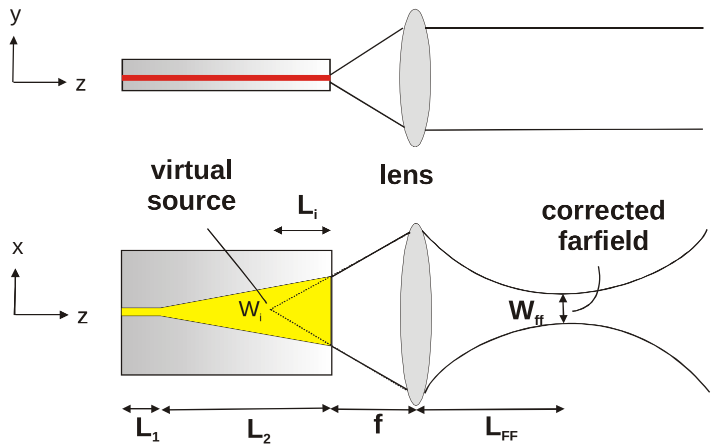

Figure 2: Schematic diagram of an astigmatism measurement. A lens is used to collimate the beam in the fast axis direction (vertically). Because of the astigmatism, the beam is focused in the lateral plane resulting in a waist, called the corrected far-field.

At the output facet the curved wavefronts of tapered diode lasers diffract according to Snell's law and the beam will propagate with a width that is approximately n_{eff} times the internal full taper angle. With a taper angle of 6° this product yields a beam about 20° wide. The beam is astigmatic, since in the direction perpendicular to the quantum well it diverges from the output facet, but in the plane of the quantum well it diverges from a virtual source that is approximately L_2/n_{eff} behind the output facet inside the device. Because n_{eff} is dependent on the carrier density and the temperature, distortions of the carrier distribution or different thermal management concepts have a remarkable influence on n_{eff} and on the position of the virtual source [14].

For the measurements, a lens is used to collimate the beam in the fast axis direction (vertically) as shown in Fig. 2. Because of the astigmatism, the beam is focused in the lateral plane resulting in a waist w_{ff}, called the corrected far-field. The distance L_{ff} between the lens and corrected far-field provides a direct measure of the astigmatism using the lens equation and the known focal length f of the measurement lens. Similarly, the width w_{ff} of the waist is a measure of the width of the virtual source.

It can also be shown that a lateral scan of the power distribution at this waist is exactly the same as the power distribution that would be found at a focal length beyond the measurement lens if an ideal thin cylindrical lens had been placed at the output facet to collimate the beam in the lateral plane (removal of the quadratic phase curvature due to the divergence of the beam).

Hence, the relative power density measured at the waist as a function of the lateral distance x is a direct measure of the far-field pattern with the quadratic phase curvature removed, if one interprets ϕ as:

$$\phi = \tan^{-1}(y/f) \tag{4}$$

This ideal beam is convenient to use as a benchmark for the beam quality of real beams. For an ideal top hat distribution the full width half maximum angle ϕ_{FWHM} for the far-field distribution of the power density is [1]:

$$\phi_{FWHM} \approx 0.84\lambda_0 / W_2 \tag{5}$$

If the near-field profile is not top hat but rather Gaussian (if gain saturation plays no role), the far-field distribution as a Fourier transformation of the Gaussian near-field distribution has a factor of 1.5 instead of 0.84 for the full width half maximum angle in equation (5).

Designing a High Brightness Tapered Diode Laser

Designing for High Output Power

For tapered diode lasers the brightness is approximately proportional to the output power divided by the beam propagation factors M^2 in the vertical and parallel directions. Therefore, one way to reach a higher brightness is to increase the output power. To illustrate the main problems of tapered diode lasers concerning the output power, a comparison [15] between a tapered laser (TL) and a broad-area diode laser (BA) is given in Table 1. The TL consists of a ridge section length of 500 µm and a tapered section length of 2 mm. The BA diode laser has a resonator length of 2 mm and a facet with of 150 µm. Both have the same vertical structure given in [16] emitting at 975 nm and the same width of the emitting facet.

	Tapered Laser	Broad-Area Laser
j_{th} (A/cm^2)	402	190
s.e. (W/A)	0.84	1.11
η_{4A} (%)	39	62
P_{4A} (W)	2.5	3.8
$J_{P,loss}$ (W/cm^2)	1820	770
α_{opt} (cm^{-1})	33.1	13.6
T_0 (K)	70	160

Table 1: Comparison of a tapered diode laser and a broad-area diode laser. The optical losses α_{opt} have been calculated from the design parameters. All values except T_0 have been measured at a heatsink temperature of 20 °C in cw operation. Both diodes have been mounted on standard c-mounts.

Two main problems are obvious: (1) Because of the additional loss mechanism of tapered diode lasers [15] the TL laser has a threshold current density which is twice the threshold current of the BA laser; (2) The thermal dissipation energy density $J_{P,loss}$ of the TL laser is also more than twice as high as for the BA laser due to the additional losses and to a smaller pumped area. Together with a dramatically reduced value for T_0 for the TL laser this leads to a higher internal laser temperature and as a consequence of this to higher threshold current and lower slope efficiency. From this point of view two concepts should be crucial to improve the output power of tapered diode lasers significantly:

1. A longer resonator length will increase the area for cooling and lower the dissipation energy density. In addition for a constant tapered angle of 6° a longer resonator length leads to a broader facet width allowing for higher output powers [16,17].
2. The thermal management plays an important role for TL lasers [14] due to the low value of T_0. Therefore it is necessary to improve the packaging in order to reduce thermal resistance.

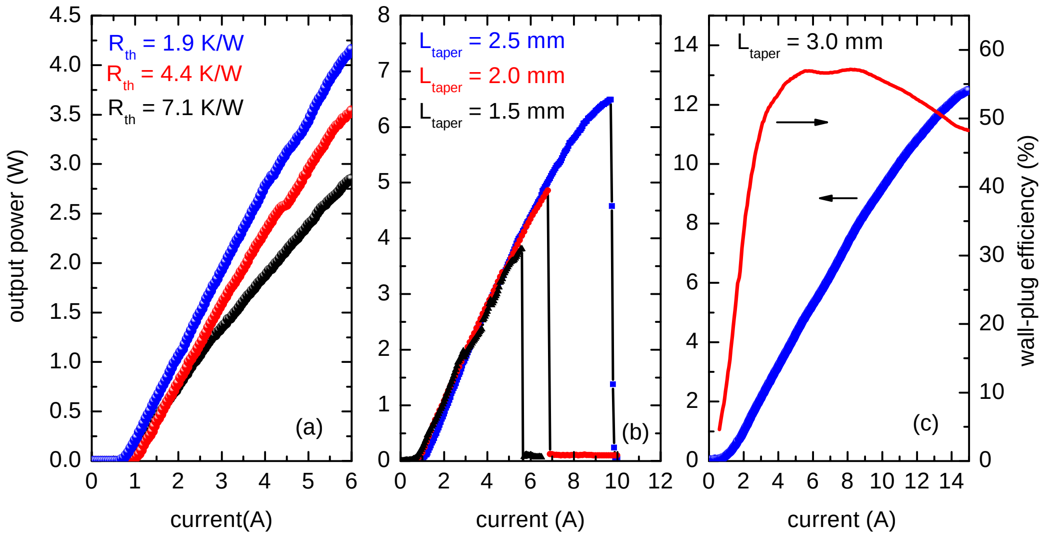

Figure 3: (a) Current-power curves for different heatsink designs. (b) Current-power curves for different lengths of the tapered section. (c) Current-power characteristic and wall-plug efficiency of a tapered diode laser with a taper section length of 3 mm and a ridge section length of 500 µm. All measurements made at a heatsink temperature of 20 °C in cw operation.

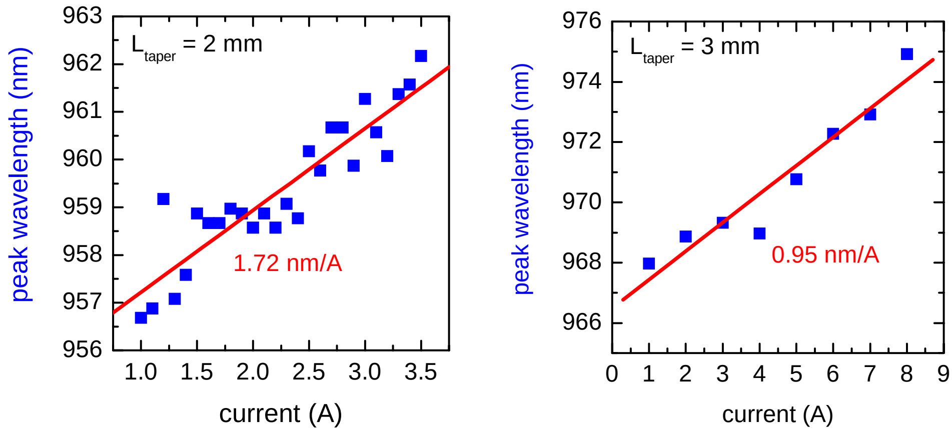

Figure 4: Peak wavelength as a function of current of tapered diode lasers with a taper section length of 2 mm (left hand side) and 3 mm (right hand side). The ridge section was 500 µm long for both lasers. The measurements have been made at a heat sink temperature of 20 °C and in cw operation.

In Fig. 3(a) some current-power curves of TL lasers with improved heatsink designs are shown. The thermal resistances can be calculated by measuring the wavelength shift with temperature and the wavelength shift with the current in pulsed mode. A thermal resistance of 7.1 K/W corresponds to the standard c-mount concept, used today for most tapered lasers. The other heatsinks are comparatively bigger copper blocks normally used for high-power broad-area diode lasers (4.4 K/W) and laser bars (1.9 K/W). As one can see, a reduction of the thermal resistance down to 1.9 K/W leads to increased output powers up to 4.2 W (at 6 A) instead of the previous 2.8 W. This means an improvement of 50% in output power only by changing the heatsink design and volume. The effect of using longer tapered sections has been demonstrated in Fig. 3(b). Taper section lengths up to 2.5 mm are shown here. There are typical currents of sudden mirror death corresponding linearly to the different facet widths of the TL lasers with the different tapered section lengths. This defines a maximum output power density of 0.025 W per µm^2 of facet area [18].

The tapered diode lasers have been characterised in terms of thermal management. Figure 4 shows the dependence of the peak wavelength on the current for lasers with a taper section length of 2 mm (left hand side) and 3 mm (right hand side). The measurements have been made at a heat sink temperature of 20 °C in cw operation. A current dependent wavelength shift of 1.72 nm/A for lasers with a 2 mm taper section length and 0.95 nm/A for lasers with a 3 mm taper section length has been measured.

From these measurements, in combination with current-power characteristics, a thermal resistance of 8 K/W has been deduced for tapered lasers with a 2 mm taper section length. By using a taper section length of 3 mm the thermal resistance has been halved to 4 K/W, impressively demonstrating the better heat dissipation in the latter case.

From the temperature dependence of the threshold current T_0 has been calculated. Whereas the laser with a 3 mm taper section length achieves a remarkably high value of (185 K ± 15 K) for T_0, lasers with a 2 mm taper section length only show values around 106 K [19].

Figure 3(c) shows the current-power characteristic together with the wall-plug efficiency for a tapered diode laser with an overall resonator length of 3.5 mm. From a fit of the data between 2 A and 4 A a comparatively low threshold current of 1.07 A corresponding to a threshold current density of 222 A/cm^2 has been deduced. The maximum slope efficiency of 1.09 W/A combined with the low series resistance of 35 mΩ results in the maximum wall-plug efficiency of 57%. This high wall-plug efficiency remains nearly constant between 6 A and 9 A corresponding to cw output powers between 5.5 W and 8.3 W. At a maximum operation current of 15 A a cw output power of 12.5 W has been obtained without COMD. Thermal rollover starts only at quite high operation currents around 9 A demonstrating the good heat dissipation due to the large area of the resonator and the low power loss of the device. The values for the wall-plug efficiency and the output power are to our knowledge the highest values in continuous wave mode for tapered diode lasers reported to date [20].

Designing for High Beam Quality

In the last section we have demonstrated that longer tapered sections lead to higher output powers. The brightness, however, will be only increased if the beam quality remains constant at these higher output powers. Therefore the influence of longer tapered section lengths on the beam quality should be analysed.

Using different lengths of ridge and taper sections can change the optical losses according to equation (3). In addition, the antireflection coating can be varied. The experimental results in Fig. 5 show that the lengths of the ridge and the taper sections have a strong impact on the beam quality at high output powers. For a ridge length of 100 µm the beam quality starts to decrease rapidly at a power level of P = 1 W. In contrast to this result, the beam quality of the devices with ridge lengths of 500 µm remain in the range of $M^2 < 1.5$ up to more than 2 W of output power. In addition, a longer taper section length also enhances the beam quality. Whereas the beam quality of devices having a taper length of 2000 µm remains nearly diffraction limited up to about 2.2 W with an M^2 value of 1.3, a taper section length of 1500 µm causes M^2 to increase rapidly above a (lower) power level of about 0.4 W. It has been shown that the increase of the length of one or both sections lowers the linewidth enhancement factor and leads to a lower tendency for filamentation and hence to a better beam quality [17].

With increasing output facet reflectivity, an increasing percentage of the optical field is reflected into the resonator enhancing the formation of dynamically varying longitudinal and transverse structures in the intensity distribution. Therefore it is reasonable to reduce the facet reflectivities as far as possible to avoid this phenomenon. In Fig. 5 antireflection coatings down to 0.005 % have been used to further improve the beam quality. However, it may be advantageous to accept higher facet reflectivities to reduce backward reflections from optical components like lenses and fibres.

Far-field profiles of the devices were measured after correcting for the quadratic phase front divergence by using a cylindrical lens (corrected far-field) according to Fig. 2. An example for the evolution of the lateral far-field profiles of tapered diode lasers with increasing output power can be seen in Fig. 6. A power independent far-field angle of 0.24 ° (FWHM) is obtained for the full range of cw output powers. This value is equal to 1.06 times the value predicted by equation (5). The fraction of power at 3 W contained inside the central lobe is 93 % (2.8 W). To estimate the brightness (P/λ^2) of this source, one can use the power in the central lobe divided by (1.06 x λ^2) where the factor 1.06 has been added to the denominator to account for the increase in the far-field angle above the diffraction limit. The result is a brightness value of 3.0×10^8 Wcm^{-2}sr^{-1} [19].

The measured M^2 parameters in Fig. 6 range between 1.1 at 1 W and 4.1 at 3 W of output power. The growth of side lobes at higher output powers is responsible for the increase of the beam quality parameter M^2. Conventionally beam diameters have been measured at the 1/e^2 intensity point; i.e. at 13.5 % of the maximum intensity. ISO 11146 requires the use of a 'Second Moment' definition of beam diameter. For this reason the side lobes also increase the calculated beam quality factor M^2.

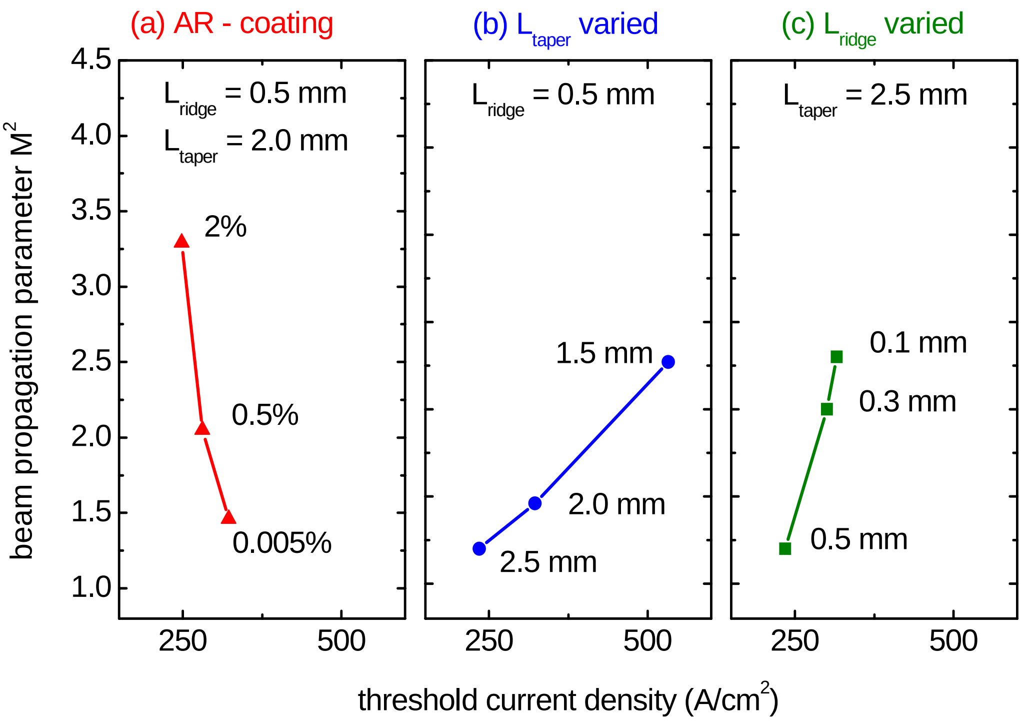

Figure 5: Typical M^2 characteristics of tapered diode lasers in dependence on the (a) antireflection coating (b) taper section length L_2 and (c) ridge section length L_1. The measurements have been made at a heatsink temperature of 20 °C and in cw mode at a power level of 1 W. All diodes have been mounted on standard C-mounts.

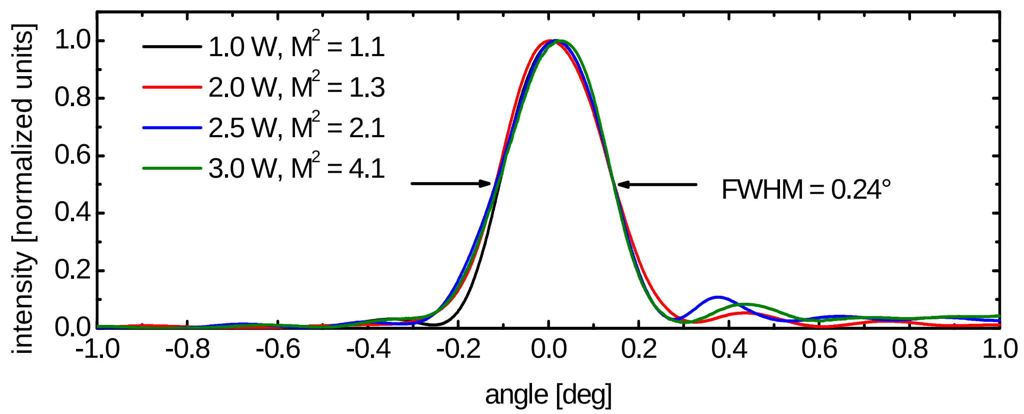

Figure 6: Dependence of the lateral far field profiles of tapered high-power diode lasers on the output power after removal of the quadratic phase curvature by a cylindrical lens at a heat sink temperature of 20 °C (cw). Additionally, the measured values of M^2 are given for each output power.

In Fig. 7 the beam propagation factors of both tapered devices with 2 and 3 mm tapered section lengths have been compared. The measurements have been made at a heat sink temperature of 20 °C in CW mode with a commercial beam analyser. The values of M^2 have been derived using two different methods: method (a) cuts the measured beam profiles at the $1/e^2$ level and uses these widths for calculating M^2; method (b) uses an integral calculation method taking into account side lobes with heights even below $1/e^2$. Normally method (b) leads to higher values of M^2. As predicted in [15] the device with the longer taper section length shows a comparatively better beam quality. For method (a) nearly diffraction-limited output powers of more than 8 W have been obtained for the longer taper section length. The value for M^2 is less than 1.4 resulting in a record value for the brightness of more than 660 MW/cm² at 8.3 W (see Fig. 8). For a taper section length of 2 mm values for the brightness around 300 MW/cm² are achievable.

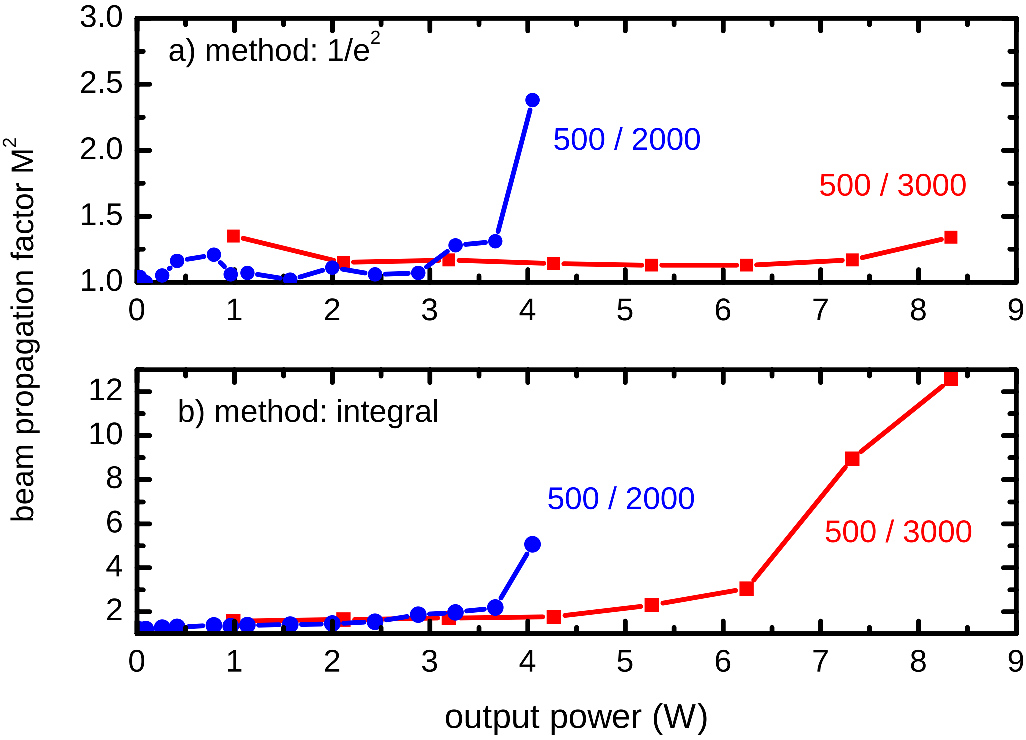

Figure 7: Beam propagation factor M^2 as a function of output power for a tapered diode laser with a resonator length of 2.5 mm (squares) and 3.5 mm (circles). The measurements have been made at a heat sink temperature of 20 °C and in CW mode with a commercial beam analyser with method $1/e^2$ (a) and with an integral measurement method (b).

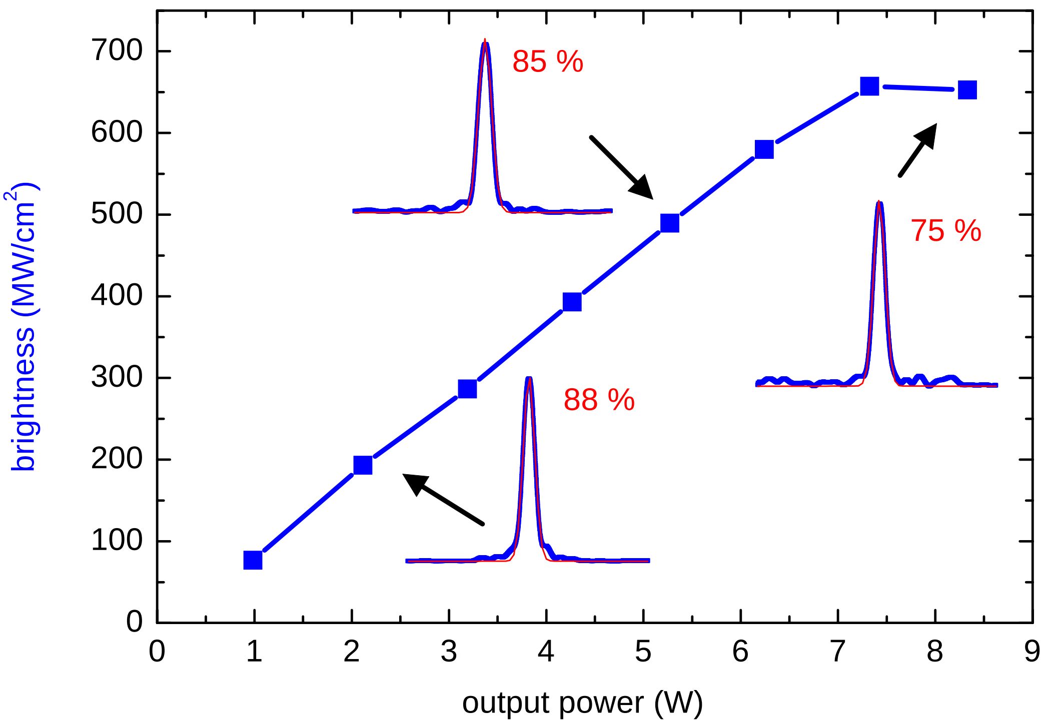

Figure 8: Brightness of a tapered laser with a 3 mm taper section length as a function of output power. The values are calculated from Figs. 2 and 7. In addition minimal beam waists are shown for 2 W, 5 W and 8.3 W. The percentage gives the fraction of output power in the central lobe of the beam waist.

Using the integral method for calculating M^2, nearly diffraction-limited values of less than 1.8 have been observed up to output powers of 4.5 W for the tapered laser with a 3 mm taper section length. The brightness is around 260 MW/cm^2 in comparison to 180 MW/cm^2 for the diode with a taper section length of 2 mm.

Finally in Fig. 8 the brightness of the tapered laser with 3 mm taper section length is shown as a function of the output power. Additionally at 2 W, 5 W and 8.3 W the measurements of the minimal beam waists are given as another quantity for beam quality. At 5 W, 85% of the output power is within the central lobe of the beam waist, and this value is still 75% at 8.3 W. In this example we have demonstrated a tapered laser with more than 6 W of diffraction-limited output power [20].

Designing for Constant Astigmatism

In Fig. 9(a) the astigmatism curves (distance between virtual source and facet) as a function of current has been investigated for different design parameters. It has been shown experimentally that in the low current regime ($I < 3I_{th}$) the ridge and the taper section length have a significant influence on the position of the virtual source, which is visible in a change of the astigmatism. There is a weaker influence of the design on the astigmatism in the higher current regime ($I > 3I_{th}$).

The astigmatism of tapered diode lasers is mainly temperature driven, as shown in Fig. 9(b). A lower thermal resistance, leading to a better heat flow, results in a fast crossover into a flat curve. In contrast to this, higher values of the thermal resistance lead to a gradual changeover to a flat behaviour. As a result, the astigmatism remains nearly constant in the higher current (higher power output) regime. The same effect takes place by making the tapered section length longer. Here for longer tapered section lengths the power losses per area decrease, there is a better heat flow, and the astigmatism reaches saturation faster.

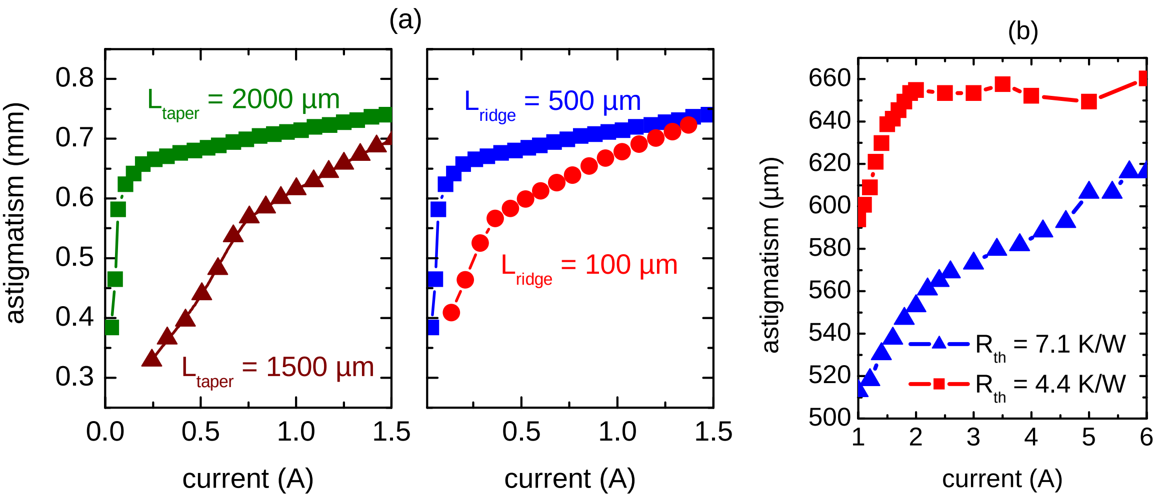

Figure 9: (a) Astigmatism of tapered diode lasers as a function of the bias current for different ridge- and tapered section lengths. All diodes have been mounted on standard c-mounts. (b) Astigmatism of tapered diode lasers emitting at 980 nm as a function of the bias current for different thermal resistances. All measurements have been made at a heatsink temperature of 20°C in cw mode. The thermal resistance has been changed by using different heatsinks.

Conclusion

In this paper we have considered the major factors affecting the brightness of tapered laser diodes and explored ways in which it can be improved. In the design optimisation we have considered three main aspects: 1) designing for high power, 2) designing for high beam quality and 3) designing for constant astigmatism. From the design optimisation, we have demonstrated tapered diode lasers with longer tapered section lengths that enable nearly diffraction-limited output powers of more than 8 W, resulting in a brightness of more than 660 MW/cm^2.

Acknowledgements

The authors gratefully acknowledge G. Bihlmann, N. Götzmann, M. Korobka, K. Schäuble and W. Fehrenbach for their technical assistance. This work was supported by the European Commission through the IST projects WWW.BRIGHT.EU (IST-511722) and WWW.BRIGHTER.EU (IST-035266).

References

[1] J.N. Walpole, “Semiconductor amplifiers and lasers with tapered gain regions” *Opt. Quantum Electron.*, **28,** 623-645 (1996).

[2] A. Moser and E.E. Latta, “Arrhenius parameters for the rate process leading to catastrophic damage of AlGaAs-GaAs laser facets” *J. Appl. Phys.*, **71,** 4848-4853 (1992).

[3] S. Pawlik, S. Traut, A. Thies, B. Sverdlov and B. Schmidt, “Ultra-high power RWG laser diodes with lateral absorber region” *18th IEEE International Semiconductor Laser Conference*, Garmisch, Germany, (2002).

[4] E.S. Kintzer, J.N. Walpole, S.R. Chinn, C.A. Wang and L.J. Missaggia, “High power strained-layer amplifiers and lasers with tapered gain regions” *IEEE Photon. Technol. Lett.*, **5,** 605-608 (1993).

[5] S. O´Brien, A. Schönfelder and R.J. Lang, “5W CW diffraction-limited InGaAs broad-area flared amplifier at 970 nm” *IEEE Photon. Technol. Lett.*, **9,** 1217-1219 (1997).

[6] S.D. de Mars, K.M. Dzurko, R.J. Lang, D.F. Welch, D.R. Scifres and A. Hardy, “Angled grating distributed-feedback laser with 1 W single-mode, diffraction-limited output at 980 nm” *Conference on Lasers and Electro-optics (CLEO)*, Anaheim, CA, U.S.A, (1996).

[7] K. Paschke, A. Bogatov, F. Bugge, A.E. Drakin, J. Fricke, R. Guther, A.A. Stratonikov, H. Wenzel, G. Erbert and G. Tränkle, “Properties of ion-implanted high-power angled-grating distributed-feedback lasers” *IEEE J. Sel. Top. Quantum Electron.*, **9,** 1172-1178 (2003).

[8] S. O´Brien, D.F. Welch, R.A. Parke, D. Mehuys, K. Dzurko, R.J. Lang, R. Waarts and D. Scifres, “Operating characteristics of a high-power monolithically integrated flared amplifier master oscillator power amplifier” *IEEE J. Quantum Electron.*, **29,** 2052-2057 (1993).

[9] A. Al-Muhanna, L.J. Mawst, D. Botez, D.Z. Garbuzov, R.U. Martinalli and C.J. Connolly, “14.3 W quasi-continuous wave front-facet power from broad-waveguide Al-free 970 nm diode lasers” *Appl. Phys. Lett.*, **71,** 1142-1144 (1997).

[10] M. Mikulla, P. Chazan, A. Schmitt, S. Morgott, A. Wetzel, M. Walther, R. Kiefer, W. Pletschen, J. Braunstein and G. Weimann, “High-brightness tapered semiconductor laser-oscillators and amplifiers with low modal gain epilayer-structures” *IEEE Photon. Technol. Lett.*, **10,** 654-656 (1998).

[11] J. Stohs, D.J. Bossert, D.J. Gallant and S.R.J. Brueck, “Gain, refractive index change and linewidth enhancement factor in broad-area GaAs and InGaAs quantum-well lasers” *IEEE J. Quantum Electron.*, **37,** 1449-1459 (2001).

[12] M. Mikulla, “Tapered high-power, high-brightness diode lasers” *Topics Appl. Phys.*, **78,** 265-288 (2000).

[13] G.C. Dente, “Low confinement factors for suppressed filaments in semiconductor lasers” *IEEE J. Quantum Electron.*, **37,** 1650-1653 (2001).

[14] R.J. Lang, A. Hardy, R. Parke, D. Mehuys, S. O´Brien, J. Major and D. Welch, “Numerical analysis of flared semiconductor laser amplifiers” *IEEE J. Quantum Electron.*, **29,** 2044-2051 (1993).

[15] M.T. Kelemen, J. Weber, S. Kallenbach, C. Pfahler, M. Mikulla and G. Weimann, “Astigmatism and beam quality of high-brightness tapered diode lasers” *Proc. SPIE*, **5452,** 233-243 (2004).

[16] M. Mikulla, M.T. Kelemen, M. Walther, R. Kiefer, R. Moritz and G. Weimann, “High-power 980 nm laser diodes by MBE” *Proc. SPIE*, **4580,** 11-18 (2001).

[17] M.T. Kelemen, J. Weber, M. Mikulla and G. Weimann, “Improved brightness using tapered diode lasers” *Conference on Lasers and Electro-optics Europe (CLEO-Europe)*, Munich, Germany, (2003).

[18] M.T. Kelemen, J. Weber, F. Rinner, J. Rogg, M. Mikulla and G. Weimann, “High-power high-brightness ridge-waveguide tapered diode lasers at 940 nm” *Proc. SPIE*, **4648,** 75-81 (2002).

[19] M.T. Kelemen, J. Weber, G. Kaufel, R. Moritz, M. Mikulla and G. Weimann, “8 W high-efficiency high-brightness tapered diode lasers at 976 nm” *Proc. SPIE*, **6104,** 61040D (2006).

[20] M.T. Kelemen, J. Weber, G. Kaufel, G. Bihlmann, R. Moritz, M. Mikulla and G. Weimann, “Tapered diode lasers at 976 nm with 8 W nearly diffraction-limited output power” *Electron Lett.*, **41,** 1011-1013 (2005).

By-Emitter Degradation Analysis of High-Power Laser Bars

S. Bull and E.C Larkins

Photonic and Radio Frequency Engineering Group, School of Electrical and Electronic Engineering, University of Nottingham, University Park, Nottingham, NG7 2RD, U.K.

Abstract

The study of degradation processes in high-power laser diodes, in particular high-power laser bars, has become increasingly important as the output power of these devices continues to rise. We present a by-emitter degradation analysis technique, which examines degradation processes at both the bar and emitter level. This technique focuses on understanding the dynamic mechanisms by which packaging-induced strain and operating conditions lead to the formation of defects and subsequent emitter and bar degradation. In one example presented, we observe a packaging-induced strain threshold above which an increase in the degradation rate is observed. In a second example, we examine a highly compressively strained bar, where thermally-induced current runaway is found to be an important factor in the bar degradation and eventual device failure.

Introduction

In recent years, rapid progress has been made in the development of high-power laser diodes for applications including pump sources for solid state lasers, materials processing and medicine. Laser bars are often used for high-power applications (>5W). As the output power of laser bars continues to increase, the degradation and reliability of such high power devices remains a critical issue. Although it is well known that laser bars degrade faster than single emitters, the reasons for this are not well understood, but seems to be related to a combination of increased (and inhomogeneous) packaging-induced stress and current competition between emitters. While many studies have looked at the reliability and degradation of single emitters, less attention has been given to understanding the details of the degradation dynamics of high-power laser bars.

A high-power laser bar can be more properly considered as an array of individual diodes connected in parallel, but sharing the same electrical connections, substrate and heatsink as shown in Fig. 1. Consequently, it is not difficult to imagine that the complex non-linear electrical, optical and thermal interactions between emitters need to be considered when investigating the degradation mechanisms of laser bars. Furthermore, the detailed nature of the degradation process in a particular device generally depends upon many factors, including: the packaging process; the quality of the epitaxial material; the detailed structure of both the emitters and the bar; and the operating conditions.

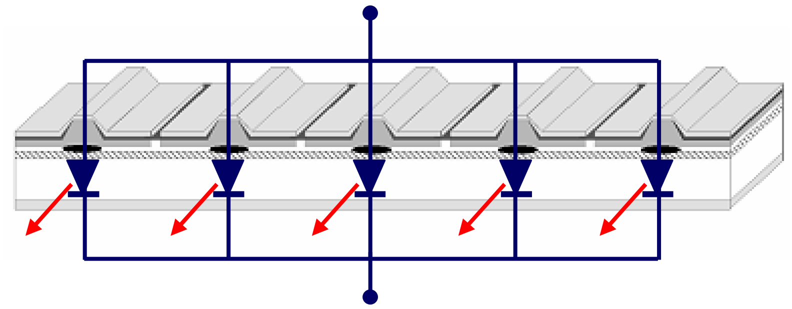

Figure 1: Layout of a high-power laser bar showing how such a bar comprises of a parallel-connected array of diodes that share the same physical connections, substrate and heatsink.

Analysis of laser bar degradation at the bar level involves measuring the integrated characteristics of the bar (e.g. total current, total output power, total output spectrum, etc.) Most aging studies carried out on laser bars (including constant power, constant current and even accelerated aging studies) are carried out at the bar level. Bar level analysis is based upon the implicit assumption that all emitters are identical and are operating under identical conditions. This assumption of identical emitter behaviour often breaks down because of inhomogeneous packaging-induced strain. Even when the packaging-induced strain is homogeneous, the assumption of identical operating conditions will begin to breakdown as the individual emitters age (statistically) at different rates. Therefore, in order to understand the degradation processes at work in a laser bar, it is necessary to understand the operating conditions of the individual emitters as completely as possible.

There have been several investigations of the properties of individual emitters within laser bars using one or two experimental methods. However, the development of the systematic by-emitter degradation approach presented here began during the NODELASE project [1] and also independently at the Max-Born-Institute [2-4] and was first clearly articulated in the POWERPACK project [5]. In our systematic by-emitter analysis, we aim to gain a better understanding of the relationship between emitter and bar degradation. The by-emitter degradation analysis technique focuses on understanding the dynamic mechanisms, by which the packaging-induced stress, current competition and individual emitter operating conditions lead to the formation of defects and subsequent emitter (and hence bar) degradation. Additionally, improved correlations can be found between the local strain, the observation of defects and the degradation of individual emitters than between these defects and degradation of the bar as a whole. Furthermore, the statistical validity of degradation studies is enhanced because of the closer relationship between local packaging-induced stress and the degradation of individual emitters. Once the specific degradation mechanism of a particular laser bar technology is understood, it is possible to optimise the reliability of this technology by specifying limits on the operating conditions or by screening the bars for particular characteristics identified by the by-emitter analysis.

In this paper, we present two specific aging scenarios that have been observed for different high-power laser bars. In some older compressively strained bars a strain threshold for device degradation was observed [6], while in other highly compressively strained bars thermal runaway was found to be the dominant degradation mechanism [7]. The investigation of these two scenarios was only made possible by the use of the by-emitter degradation analysis methodology. The by-emitter experimental techniques used are also discussed.

Experimental Techniques

A wide range of experimental techniques can be employed for by-emitter degradation studies. Table 1 summarises the techniques used in the two studies presented in this paper. Table 1 also lists the quantities measured when performing each technique and what each of these quantities is sensitive to. Each of these techniques is then described briefly and the reader is referred to the various references listed for further detailed information. Finally, at the end of this section, the analysis of by-emitter measurement data is discussed.

Technique:	Quantities measured:	Sensitive to:	Refs:
Micro-Photoluminescence (μ-PL)	E_g in centre of substrate (can also be measured at QW)	Packaging-induced strain	[8-10]
Photocurrent Spectroscopy (PCS)	QW transition energies, E_g of the waveguide	Packaging-induced strain, Electric field	[3,4,11]
Laser Beam Induced Current (LBIC)	Sub-bandgap absorption	Defects, Shifts in absorption edge	[11,12]
Photoluminescence Microscopy (PLM)	Defects	Non-radiative recombination centres	[13-15]
Electroluminescence Microscopy (ELM)	Defects, Absolute & relative emitter power, $I_{th\text{-}i}$, $\eta_{app\text{-}i}$	Non-radiative recombination centres, Temperature, ΔE_g, Scattering loss, η_{int}	[16,17]
Near-Field Spectra (NFS)	Defects, $\Delta\lambda/\Delta I$	Non-radiative recombination centres, Temperature, Quasi-Fermi level separation	[16,17]

Table 1: Summary of by-emitter experimental techniques and the quantities measured.

Definitions

Whilst many of the parameters in Table 1 (e.g. bandgap, wavelength and power) can be measured locally for each emitter, it is not possible to determine the currents of individual emitters due to the nature of the bar (i.e. a parallel-connected array of emitters sharing the same anode and cathode). With this configuration, it is only possible to measure the total bar current. For the purpose of by-emitter analysis, two quantities related to the performance of individual emitters can be defined [6,18]. These new quantities are the "apparent" threshold current of the i_{th} emitter I_{th_i} and the "apparent" external differential quantum efficiency of the i_{th} emitter η_{app_i}. These quantities are determined from the P_i-vs-I_{BAR} curves of individual emitters, where P_i is the power of an individual emitter, but the current I_{BAR} is that of the total bar.

Micro-Photoluminescence Spectroscopy

Micro-photoluminescence spectroscopy (μ-PL) is widely used to measure packaging-induced strain, which is caused during the soldering of a laser bar to a heatsink. This process can introduce an inhomogeneous strain profile across a device and is known to play a role in defect formation and affect device reliability [8-10]. μ-PL linescans can be simply performed by measuring PL spectra at points across the substrate of a laser bar at a position that is in the centre of the substrate (~50 μm from the active region). With knowledge of the bar geometry (i.e. the number of emitters, the emitter width and the emitter pitch), an average value of the peak PL wavelength can be calculated for each individual emitter together with the change in peak PL wavelength across an individual emitter. Through the electronic deformation potentials, these PL spectral shifts can be converted to local stress values and the strain can be determined as being either compressive or tensile.

Laser Beam Induced Current

Laser beam induced current (LBIC) is a relatively simple technique, which is sensitive to the presence of defects [11,12]. Normally two scans are made across the facet of a laser bar. The first of these is commonly performed using a He-Ne laser (632.8 nm) and is used for alignment purposes. The second scan uses a wavelength below the bandgap of the material of the laser that is being characterised. For this technique to be effective, the laser wavelength used for scanning the device must be selected to be just below the band edge of the material. For 808 nm lasers, an appropriate scanning wavelength is 830 nm (semiconductor laser) and for 980 nm lasers, an appropriate scanning wavelength is 1064 nm (Nd:YAG laser). In the case of 808 nm bars, the LBIC excitation signal is closer to the QW bandgap energy than it is for 980nm bars, so in this case the LBIC signal is sensitive to changes in both the bandgap energy and the slope of the band edge. In an LBIC measurement, the monochromatic excitation of the active region is scanned along the width of the laser bar. As with μ-PL linescans, the intensity of the LBIC signal at the centre of each emitter can be found using knowledge of the bar geometry (i.e. the number of emitters, the emitter width and the emitter pitch).

Photocurrent Spectroscopy

Photocurrent spectroscopy (PCS) is sensitive to optical absorption processes in semiconductor optoelectronic devices [3,4,11]. The principle of the PC measurement is to illuminate the sample with light at a given wavelength and measure the current generated by the recombination of electron-hole pairs. A PCS spectrum is related to the absorption spectrum of the active region of a laser diode. This allows the extraction of information about the band structure of the materials that make up the quantum well and the cladding regions. When performing a by-emitter analysis, a PC spectrum is measured at the centre of each emitter in a laser bar. From the spectra, the first derivative is calculated and this allows the spectral position of the lowest quantum-confined transition in the quantum well to be determined for each emitter.

Photoluminescence Microscopy

Photoluminescence microscopy (PLM) is a powerful imaging technique for studying defects and degradation in semiconductor materials and devices [13-15]. The power of the PLM technique is due to the intrinsic sensitivity of optical processes to the presence of defects. PLM is non-destructive, offers nearly diffraction limited spatial resolution and is very sensitive to non-radiative defects. In laser bars, defects usually appear as dark features in the luminescence images, but bright features can also be observed. Defects are observed in both the active region and substrate by visual inspection of the PLM images and, for the purposes of by-emitter analysis, these defects are logged on a by-emitter basis.

Electroluminescence Microscopy

Electroluminescence microscopy (ELM) complements PLM in the identification of defects and inhomogeneities in the luminescence from individual emitters. ELM is also sensitive to defects that are inside the cavity (i.e. not just at the facets) [13,16]. Furthermore, ELM investigations of individual emitters at a range of bias currents (both above and below threshold) can provide further information, such as the emitters' absolute and relative power, their apparent threshold current and their apparent external differential efficiency. Changes in these parameters are related to changes in temperature, bandgap energy, internal efficiency and absorption and scattering losses, as listed in Table 1, and provide important information for understanding the operating conditions and performance of the individual emitters as well as the variation in these operating conditions within a laser bar.

Near-Field Spectra

The near-field spectra of individual emitters provide information on defects through either the visual observation of inhomogeneities in the spectra or by using a fast Fourier transform (FFT) analysis technique [16,17,19,20]. If spectra are measured at a range of bias currents, the wavelength shift as a function of current for individual emitters can be determined. This is related to device temperature changes (if the emitter is above threshold) and shifts in the quantum well quasi-Fermi level separation (if the emitter is below threshold).

By-Emitter Data Analysis

The wide range of techniques presented, when used to make by-emitter measurements, can provide a large amount of information about the operation and degradation of a bar. Although by-emitter degradation analysis is still relatively new, it has been found useful to plot the data obtained from by-emitter measurements in two ways. Firstly, results are plotted as a function of emitter number or lateral position along the laser bar. This reveals: (1) the strain profile along the packaged bar; (2) differences between the performance of emitters in the centre and at the edges of the bar; (3) individual emitters whose performance differs from those around it (e.g. due to defects); and (4) if there is an asymmetry associated with the bar or the packaging (soldering) process. Secondly, results are plotted as a function of the peak wavelength of the PL spectra from the GaAs substrate beneath each emitter, which is used a measure of the local packaging-induced strain. As previously described, packaging-induced strain has been found to play a role in the degradation of laser bars.

Study 1: Observation of a Packaging-Induced Strain Threshold

In the first case study presented, a range of by-emitter analysis techniques were used to investigate 808 nm AlGaAs/GaAs high power laser bars. This study revealed the existence of a strain threshold for device degradation in this particular bar technology [6].

Experimental Details

The devices investigated were 808 nm AlGaAs GRINSCH SQW laser bars, grown by MOCVD on (100) n-type GaAs substrates. The chip dimensions were ~100 µm (bar thickness) x 900 µm (cavity length) x 1 cm (total lateral width). Each bar contained 27 emitters, each 200 µm wide. These bars were mounted epitaxial-side down onto Cu heatsinks with In solder. The bars were then aged for 700 hours under constant injection current conditions. In this investigation, strain profiles were determined from µ-PL linescans, while PLM and ELM were used to observe mirror facet defects. ELM images from the output facets of the individual emitters were observed as a function of the total bar current, allowing the determination of the apparent threshold current and the apparent external differential quantum efficiency of each individual emitter. Furthermore, PCS was performed to investigate the shift of the absorption band edge and the strength of sub-bandgap absorption.

Defects and Emitter Performance

Figure 2 shows the peak position of the µ-PL spectra as a function of the position along a device designated as ‘Bar 1’. The horizontal dotted line represents the position of the strain-free peak emission energy, as determined from measurements on an unmounted bar from the same batch. The material is compressively strained when the peak PL energy is above this line. The vertical lines at the bottom of Fig. 2 indicate the positions of mirror facet defects observed by PLM or ELM, while the shaded rectangles represent the regions where a number of defects are observed. Most of these defects appear in regions of high compressive strain, consistent with the supposition that these defects serve to relax the packaging-induced strain.

Figure 3(a) shows the integrated ELM intensities of selected emitters from Bar 1 as a function of the total bar current. The apparent external differential quantum efficiencies and the apparent threshold currents of all the individual emitters from two laser bars with identical structures were determined from plots similar to this. A comparison of the slope of the integrated ELM intensities demonstrates that emitters in the regions of higher compressive strain have higher apparent threshold currents and lower apparent external differential quantum efficiencies. PCS measurements were performed on individual emitters to investigate the effect of the strain on the QW absorption band edge. Figure 3(b) shows the PC spectra obtained from selected individual emitters from Bar 1, together with the broad-area PC spectrum obtained by exciting the entire laser bar. The photocurrent spectra from emitters located in regions of higher strain (e.g. emitter numbers 3 & 24) display reduced absorption edge slopes and larger PC tails in the sub-bandgap region than those of the strain free emitter (emitter number 8). This suggests that the larger tails of the PC spectra can be attributed to a stronger absorption of defects in the active region.

Point defects or dislocations can initially be created in the active region during crystal growth or during the mounting procedure, serving as nucleation sites for the formation of defect complexes. The relaxation of packaging-induced stress provides a driving force for the propagation of dislocation/defect complexes, which leads to increased sub-bandgap absorption.

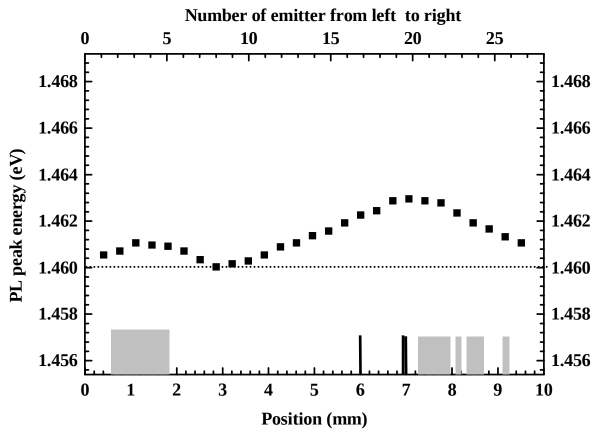

***Figure 2:** μ-PL peak position as a function of position along Bar 1. Positions where defects were observed are marked with a vertical black line, while regions where a number of defects were observed are marked by a shaded rectangle.*

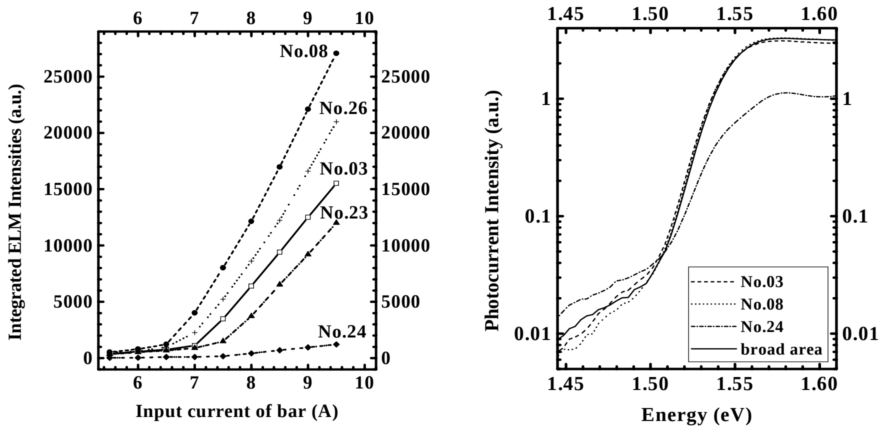

***Figure 3:** Selected emitters in bar 1, (a) Integrated intensities of the near field patterns as a function of the total bar current, (b) Normalized PC spectra shown together with the broad-area PC spectrum measured from the entire bar.*

Observation of a Strain Threshold

Figure 4 shows the apparent external differential quantum efficiency (η_{app}) and the apparent threshold current (I_{th}) and the results of PC measurements as a function of PL peak position (a measure of packaging-induced strain) for two bars with identical structures and packaging processes. A strain threshold for the degradation of the emitter performance can be seen at the PL emission energy of 1.4609 eV. The vertical dotted line at 1.4600 eV represents the strain-free condition and the shift of emission energy from 1.4600 eV to 1.4609 eV corresponds to a compressive stress of 8.4 MPa. During the initial stage of strain increase, i.e. for emitters below the 1.4609 eV threshold, there are no significant changes in the η_{app} and I_{th} of these emitters as shown in Figs. 4(a) and 4(b). However, as the strain increases beyond the PL emission energy of 1.4609 eV, η_{app} decreases and I_{th} increases for emitters in both bars with further increases in strain. Figure 4(c) also shows that I_{PC} (850 nm) increases significantly at this stage, suggesting that stronger sub-bandgap optical absorption occurs in these regions. A comparison of Figs. 4(a), 4(b) and 4(c) reveals that the degradation of devices can be attributed to the formation and accumulation of defect complexes with the strain increasing to a critical value. The propagation of defect complexes increases the density of nonradiative recombination centres in the active region. Similar strain-relaxation/degradation mechanisms have also been observed in strained InGaAs/GaAs MQW lasers. Figure 4(d) reveals an inverse correlation between compressive strain and the magnitude of $(dI_{PC}/dE)|_{max}$. There are two possible explanations for the decrease of the $(dI_{PC}/dE)|_{max}$, both of which may play a role. The first explanation is that defect formation in the highly strained regions causes an increase in sub-bandgap absorption in this region.

This would also explain why laser degradation occurs in regions of high optical power during laser operation. The second possible explanation is that the bandgap absorption edge is broadened by inhomogeneous strain. In Fig. 4(e), the position of $(dI_{PC}/dE)|_{max}$ displays a blue shift of the bandgap absorption edge over the entire range of the increased compressive strain, which is a consequence of the fact that the quantum well is also strained.

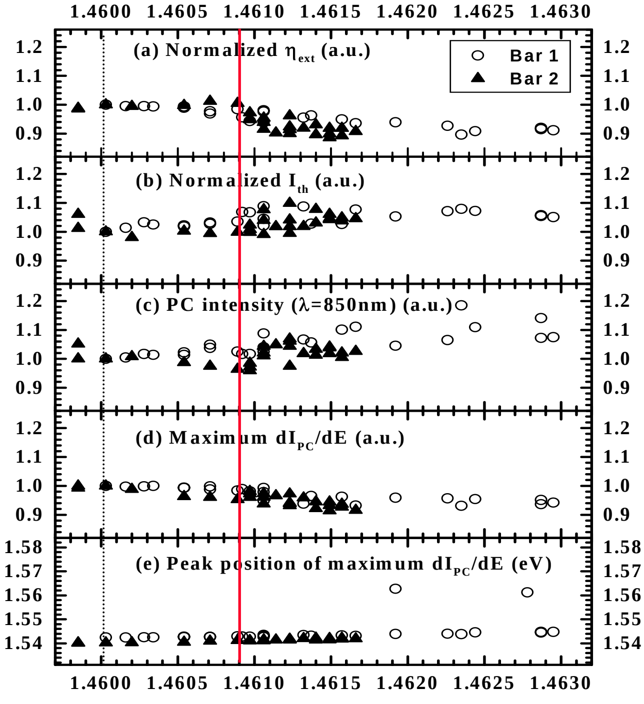

***Figure 4:** By-emitter measurements as a function of PL peak position: (a) Apparent external differential quantum efficiencies η_{app}; (b) Apparent threshold currents I_{th}; (c) Photocurrent intensities I_{PC} at λ = 850 nm; (d) The magnitudes of the first derivative $(dI_{PC}/dE)|_{max}$ of the PC spectra; and (e) The peak positions of $(dI_{PC}/dE)|_{max}$.*

Study 2: Dominant Degradation Mechanism of Thermal Runaway

In the second case study presented, a range of by-emitter analysis techniques were again used to investigate 808 nm AlGaAs/GaAs high power laser bars. Additionally common parameters (power, wall plug efficiency, threshold current, slope efficiency) of the whole bar were also monitored during the aging tests (we refer to these as conventional aging results to distinguish them from the by-emitter measurements). In this study, the dominant degradation mechanism was found to be thermally-induced current runaway [7].

Experimental Details

The high power laser bar studied here was a 1 cm wide, 808 nm AlGaAs/GaAs device grown by MOVPE and designed for 30-40 W CW operation. The bar contained a linear array of 25 emitters, which were 200 µm wide, 900 µm long and separated by 200 µm isolation regions. The bar was mounted with the epitaxial side directly soldered onto an actively cooled Cu heatsink with In solder. It was aged under CW constant current conditions for 100 hours (the burn-in period) followed by two aging periods of 500 hours each. The initial facet load for the burn-in period and the first 500 hours of aging was 10 mW/µm and this was increased to 12 mW/µm for the second 500 hours of aging.

Conventional Aging Results

Figure 5 shows the conventional aging results for the bar studied. Figure 5(a) shows there was no power loss during the burn-in period and only a 1.4% decrease during the first 500 hour aging period. However, catastrophic degradation occurred in the first few hours of the second 500 hour aging period, resulting in a power loss in excess of 70%. As the bar degrades over time, an increase in threshold current, a decrease in wall plug efficiency and a decrease in slope efficiency were all observed (see Figs. 5(b), 4(c) and 4(d), respectively). (Note that the spike at 600 hours in Fig. 5(a) is an artefact caused by the bar being removed and replaced in the aging rack.)

From this type of standard electro-optical characterisation during aging tests it is possible to classify the main degradation mode as "gradual", "rapid" or "catastrophic" – in this bar, gradual during the first aging phase followed by catastrophic in the second aging phase. However, it is not possible to determine from these simple tests, the exact cause of the degradation or where in the device it occurred. This is the primary goal of the by-emitter degradation analysis technique.

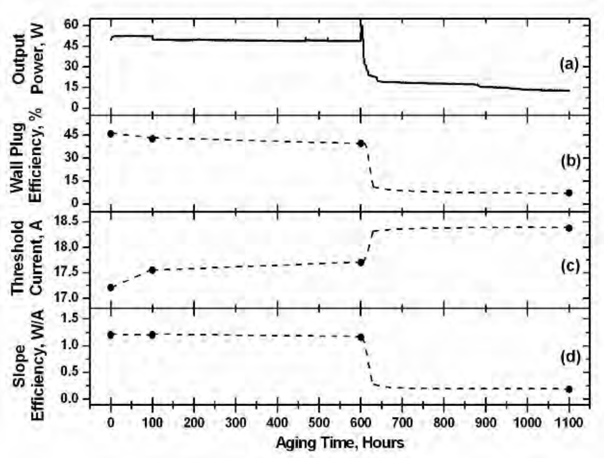

Figure 5: Conventional aging characteristics: (a) Power, (b) Wall plug efficiency, (c) Threshold current, (d) Slope efficiency. The spike at 600 hours in (a) is an artefact of the measurement as the bars was removed from the aging rack, measured and then replaced. The dashed lines in (b)-(d) indicate the expected trends in these quantities based on the power-time dependence in (a).

By-Emitter Results and the Thermal Runaway Model

Figure 6 shows the results of the by-emitter measurements from this device as a function of emitter number. Figure 6(a) shows that the bar is compressively strained in the centre after initial aging to 600 hours. With the exception of the last 5 emitters at the right hand end of the bar, further aging to 1100 hours does not cause a dramatic difference in the shape of the strain profile, although gradual strain relaxation is observed near the centre of the bar. The large increase in the μ-PL profile for the last five emitters is not a real change in strain, but is caused by a loss in the μ-PL signal strength, where the facet suffered catastrophic degradation. (Facet melting in this region was confirmed by visual inspection.)

Figure 6(b) shows that the LBIC intensity profile measured by excitation just below the band edge has a similar shape to the strain profile. This is not unreasonable, since the LBIC signal of 808 nm lasers is sensitive to changes in the bandgap when measured using an 830 nm excitation source. Such bandgap changes can be caused by strain. Figure 6(c) shows that the bandgap for the emitters at the edges of the bar is lower than that of those in the centre. This may be due to the lower value of strain at the edges of the bar. The different bandgaps for the different emitters will clearly cause small variations in the turn-on voltages (and more significant variations in the operating currents) of the emitters.

Figures 6(d) and 6(e) show the apparent threshold currents and apparent external differential efficiencies for each emitter, respectively. As with the previous data, clear differences are seen between the emitters at the edges of the bar and those in the centre. Emitters near the centre of the bar have lower I_{th} and higher η_{app} than those towards the edges. Again, the last few emitters at the right hand end of the bar (i.e. those which subsequently suffered catastrophic degradation) show anomalous behaviour.

Figure 6(f) shows the wavelength shift as a function of bias current for each emitter. Here this wavelength shift was determined below the lasing threshold and is therefore primarily a measure of the quasi-Fermi level separation (i.e. band filling of the QW) rather than a measure of the junction temperature. (When a laser diode is operated above threshold, it is usually assumed that the quasi-Fermi levels are pinned and the resulting wavelength shift is often used as a measure of the change in the average junction temperature.) A larger negative wavelength shift with increasing bias current is observed for the emitters at the edges of the bar compared to those in the centre, suggesting that the current in the emitters at the edges is increasing faster in these emitters than that of those emitters in the centre.

Figure 6(g) shows the power from each emitter measured at 20 A (~2.5 A above threshold). A clear variation is observed across the bar, with the emitters towards the edges of the bar emitting up to 2.5 times less power than those at the centre of the bar. This is consistent with the observed increase in I_{th} and the decrease in η_{app} of the emitters at the bar edges and suggests that the emitters at the edges are hotter and/or suffer from increased non-radiative recombination losses. Whilst a temperature distribution with a minimum in the centre of the bar contradicts previously observed results for both actively and passively cooled bars, this is true only of the bulk temperature. Facet temperature measurements made using Raman spectroscopy on similar devices have revealed that a temperature distribution where the facet temperature is higher at the end of the bar can occur in aged devices. This increase in temperature may be due to an increased number of non-radiative recombination centres in the emitters towards the ends of the bar or increased surface currents at the edges of the bar. Additionally, the power is seen to begin to rise again in the last three emitters at the right hand end of the bar. These emitters later suffered catastrophic damage (facet melting) during the second aging period.

The exact causes of the defects in this bar are unclear and would require further investigation. Defects may have been introduced during packaging (i.e. mechanical damage) or may be caused by the increased emitter currents (resulting from a lower bandgap energy) or by the higher surface currents at the edges of the bar. However, any increased non-radiative recombination caused by defects will lead to increases in emitter current and temperature, thereby forming a positive feedback mechanism to enhance defect generation and propagation. This ultimately leads to thermal/defect-induced runaway of the emitter current and the onset of a rapid degradation mechanism - as was observed during the further aging of this bar.

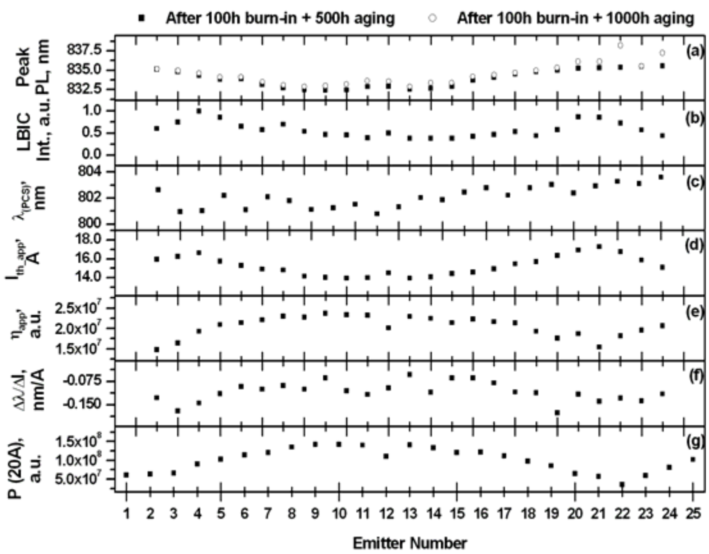

Figure 6: Emitter performance as a function of emitter number (or position along the bar): (a) Peak PL wavelength; (b) LBIC intensity; (c) QW bandgap energy; (d) Apparent threshold current I_{th}; (e) Apparent external differential efficiency η_{app}; (f) Slope of the injection-induced shift in emission wavelength $\Delta\lambda/\Delta I$; and (g) Relative emitter power at 20 A.

By-Emitter Results and Packaging-Induced Strain

As described previously, by-emitter results can also be plotted as a function of peak PL wavelength from the substrate, which is used as a measure of packaging-induced strain. Figure 7 shows the by-emitter results plotted in this way. Note that the compressive strain increases from right to left in these graphs, since the horizontal axes are plotted in nanometres. Figure 7(a) shows a limited correlation between the LBIC intensity and strain. This is likely to be due to the fact that the LBIC technique is sensitive not only to strain, but also to defects. Figure 7(b) shows that there is a direct relationship between the energy of the lowest QW-transition and the level of strain, with emitters that are more compressively strained having a larger QW transition energy. This shows that µ-PL and PCS provide similar information about the packaging-induced strain - the only difference is the position where the measurement is made (at the centre of the substrate for µ-PL and at the active region for PCS). Figures 7(c) – 7(f) all show clear correlations with strain, with emitters that are more compressively strained (i.e. in the bar centre) having a lower apparent threshold current, a higher external differential efficiency, a smaller wavelength shift as a function of sub-threshold bias current and a higher output power.

In the first case study presented, a packaging-induced strain threshold was found to exist, above which an increase in the rate of degradation during operation is observed. From the graphs shown in Fig. 7, it can be seen that no such threshold was observed for this device. However, this device is highly compressively strained with ~3 nm variation in peak PL wavelength from bar centre to edge and it is therefore possible that all of the emitters measured from this bar are strained above the threshold value observed at ~0.5 nm above the strain free condition in the first case study.

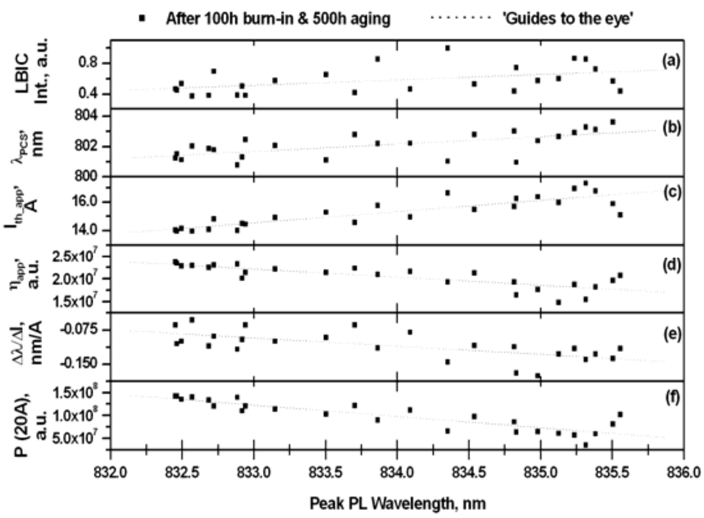

Figure 7: Emitter performance characteristics as a function of the substrate peak PL wavelength (a measure of packaging-induced strain): (a) LBIC intensity; (b) QW bandgap energy; (c) Apparent threshold current I_{th}; (d) Apparent external differential efficiency η_{app}; (e) Slope of the injection-induced shift in emission wavelength $\Delta\lambda/\Delta I$; and (f) Relative emitter power at 20 A. (Note: The amount of compressive strain increases from right to left.)

Conclusion

We have presented a by-emitter analysis method for investigating degradation in high power laser bars. By looking at degradation processes at the bar and emitter level, a better understanding can be gained of the relationship between emitter and bar degradation. The by-emitter degradation analysis technique focuses on understanding the dynamic mechanisms by which the packaging-induced stress, current competition and emitter operating conditions lead to the formation of defects and subsequent emitter (and hence bar) degradation.

We have presented two specific examples that demonstrate the value of the extra information and considerable insight gained by performing this type of by-emitter analysis. In the first example presented, the degradation process for a compressively strained bar was observed to have a packaging-induced strain threshold, above which rapid emitter degradation occurred. In the second example presented, a highly compressively strained bar was investigated and the by-emitter results showed that the predominant degradation mechanism was thermally-induced current runaway. Both of these examples successfully demonstrate the advantages of by-emitter analysis compared to the standard electro-optical aging studies of whole laser bars. These results also confirm that measurement and control of packaging-induced strain is important in laser bar fabrication and processing and in doing so it is possible to achieve significant improvement in the degradation behaviour of these devices.

Current work in the WWW.BRIGHTER.EU project will apply the by-emitter methodology to red-emitting laser bars and laser bars mounted on both standard and on expansion-matched heatsinks. Red-emitting lasers are well-suited for this kind of study because they suffer from rapid degradation, while expansion-matched heatsinks are of interest to study because of the established links between packaging-induced strain and bar degradation.

Acknowledgements

The authors gratefully acknowledge the important contributions of A.V. Andrianov, K. Boucke, I. Harrison, J.P. Landesman, J. Nagle, M. Oudart, C. Scholz, J.W. Tomm and R. Xia in providing measurements and devices to this work. This work was supported by the European Commission through the IST projects POWERPACK (IST-2000-29447), WWW.BRIGHT.EU (IST-511722) and WWW.BRIGHTER.EU (IST-035266).

References

[1] NODELASE *"Non destructive laser diode screening and evaluation"* EC Contract No. BE-1945/BRPR-0029 (1997-2000).

[2] R. Puchert, J.W. Tomm, A. Jaeger, A. Barwolff, J. Luft and T.W. Spath, "Emitter failure and thermal facet load in high-power laser diode arrays" *Appl. Phys. A*, **66**, 483-486 (1998).

[3] J.W. Tomm, R. Muller, A. Barwolf, T. Elsaesser, D. Lorenzen, F.X. Daiminger, A. Gerhardt and J. Donecker, "Direct spectroscopic measurement of mounting-induced strain in high power optoelectronic devices" *Appl. Phys. Lett.*, **73**, 3908-3910 (1998).

[4] J.W. Tomm, R. Müller, A. Bärwolf, T. Elsässer, A. Gerhardt, J. Donecker, D. Lorenzen, F.X. Daiminger, S. Weiss and M. Hurter, "Spectroscopic measurement of packaging-induced strains in quantum-well laser diodes" *J. Appl. Phys.*, **86**, 1196-1201 (1999).

[5] POWERPACK *"Screening and packaging techniques for highly reliable laser bars for telecommunication and industrial applications"* EC Contract No. IST-2000-29447 (2001-2003).

[6] R. Xia, E.C. Larkins, I. Harrison, S.R.A. Dods, A.V. Andrianov, J. Morgan and J.P. Landesman, "Mounting-induced strain threshold for the degradation of high-power AlGaAs laser bars" *IEEE Photon. Technol. Lett.*, **14**, 893-895 (2002).

[7] S. Bull, J.W. Tomm, M. Oudart, J. Nagle, C. Scholz, K. Boucke, I. Harrison and E.C. Larkins, "By-emitter degradation analysis of high power laser bars" *J. Appl. Phys.*, **98**, 063181 (2005).

[8] P. Martin, J.P. Landesman, R. Bisaro, E. Martin, A. Fily and J.P. Hirtz, "Packaging-induced stress distribution in high power AlGaAs laser diodes by PL mapping" *Mat. Sci. Eng.*, **B80**, 188-192 (2001).

[9] J.P. Landesmann, "Micro-photoluminescence for the visualisation of defects, stress and temperature profiles in high-power III–V's devices" *Mat. Sci. Eng.*, **B91-92**, 55-61 (2002).

[10] E. Martin, J.P. Landesman, J.P. Hirtz and A. Fily, "Micro-photoluminescence mapping of packaging-induced stress distribution in high power AlGaAs laser diodes" *Appl. Phys. Lett.*, **75**, 2521-2523 (1999).

[11] J.W. Tomm, A. Gerhardt, D. Lorenzen, P. Hennig and H. Roehle, "Diode laser testing by taking advantage of its photoelectric properties" *Proc. SPIE*, **4648**, 9-21 (2002).

[12] J.W. Tomm, A. Barwolff, A. Jaeger, T. Elsaesser, J. Bollmann, W.T. Masselink, A. Gerhardt and J. Donecker "Deep level spectroscopy of high-power laser diode arrays" *J. Appl. Phys.*, **84**, 1325-1332 (1998).

[13] A.V. Andrianov, S.R.A. Dods, J. Morgan, J.W. Orton, T.M. Benson, I. Harrison, E.C. Larkins, F.X. Daiminger, E. Vassilakis and J.P. Hirtz, "Optical and photoelectric study of mirror facets in degraded high power AlGaAs 808 nm laser diodes" *J. Appl. Phys.*, **87**, 3227-3233 (2000).

[14] Z.M. Wang, M. Baeumler, W. Jantz, K.H. Bachem, E.C. Larkins and J.D. Ralston, "PL microscopy investigation of lattice defects in epitaxial heterostructures" *J. Cryst. Growth*, **126**, 205-215 (1993).

[15] M. Baeumler, J.L. Weyher, S. Müller, W. Jantz, R. Stibal, G. Herrmann, J. Luft, K. Sporrer and W. Späth, "Investigation of degraded laser diodes by chemical preparation and luminescence microscopy" *Inst. Phys. Conf. Ser.*, **160**, 467-470 (1997).

[16] R. Xia, A.V. Andrianov, S. Bull, I. Harrison, J.P Landesman and E.C. Larkins, "Micro-electroluminescence spectroscopy investigation of mounting-induced strain and defects on high power GaAs/AlGaAs laser diodes" *Opt. Quantum Electron.*, **35**, 1099-1106 (2003).

[17] P.J. Bream, S. Bull, I. Harrison, S. Sujecki and E.C. Larkins, "Fourier transform analysis method for modeling the positions and properties of cavity defects in Fabry-Pérot laser diodes" *Appl. Phys. Lett.*, **86**, 061104 (2005).

[18] R. Xia, E.C. Larkins, I. Harrison, S.R.A. Dods, A.V. Andrianov, J. Morgan and J.P. Landesman, "The effect of mounting induced strain and defects on the properties of AlGaAs 808nm laser diode" *Synthetic Metals*, **127**, 255-259 (2002).

[19] A. Klehr, G. Beister, G. Erbert, A. Klein, J. Maege, I. Rechenberg, J. Sebastian, H. Wenzel and G. Tränkle, "Defect recognition via longitudinal mode analysis of high power fundamental mode and broad area edge emitting laser diodes" *J. Appl. Phys.*, **90**, 43-47 (2001).

[20] P. Lambkin, C. Percival and B. Corbett, "Reflectivity measurements of intracavity defects in laser diodes" *IEEE J. Quantum Electron.*, **40**, 10-17 (2004).
